Journal of Cleaner Production 553 (2026) 148033

Contents lists available at ScienceDirect

Journal of Cleaner Production

journal homepage: www.elsevier.com/locate/jclepro

Sustainable and economical intelligent management of urban energy communities with prosumers

Pablo Horrillo-Quintero [a,c], Pablo García-Triviño [b], Mohammad Sadegh Javadi [c], Luis M. Fernández-Ramírez [b,*], João P.S. Catalão [c]

[a] Research Group in Sustainable and Renewable Electrical Technologies (PAIDI-TEP023), Department of Electrical Engineering, ESI Puerto Real, University of Cadiz, Avda. Universidad de Cadiz, n○ 10, Puerto Real, 11519, Cadiz, Spain
[b] Research Group in Sustainable and Renewable Electrical Technologies (PAIDI-TEP023), Department of Electrical Engineering, Higher Technical School of Engineering of Algeciras (ETSIA), University of Cádiz, Avda. Ramón Puyol, s/n., Algeciras, 11202, Cadiz, Spain
[c] Research Center for Systems and Technologies (SYSTEC), Advanced Production and Intelligent Systems Associate Laboratory (ARISE), Faculty of Engineering, University of Porto, 4200-465, Porto, Portugal

HIGHLIGHTS

- Fuzzy logic controlled adaptive model predictive control for energy communities with prosumers.
- New bi-layer architecture manages conflicting energy objectives.
- Fuzzy logic supervisor computes real-time optimal cost function weights.
- Achieved 18.25% cost reduction and 25.91% less grid dependency.
- Strategy enables resilient and efficient future energy system operations.

ARTICLE INFO

Keywords:
Demand-side management
Energy communities
Prosumers
Renewable energy utilisation
Intelligent management

ABSTRACT

The transition to sustainable urban energy systems relies on the effective operation of renewable-based Energy Communities (ECs). However, a critical challenge persists: managing their dynamic operation to simultaneously minimise costs, maximise self-sufficiency, and reduce energy losses. Fixed, compromised control methodologies often fail to balance these conflicting objectives, leading to economic inefficiency and curtailing clean energy. This paper proposes a novel intelligent management framework designed to overcome this challenge. The framework is built on a bi-layer control architecture that synergistically combines a high-level fuzzy logic (FL) supervisor with an adaptive model predictive control (AMPC). The FL supervisor acts as a strategic layer, leveraging dynamic grid prices and available reserve power to perform demand-side management and compute adaptive weights for the AMPC. The AMPC layer translates this high-level strategy into optimal, predictive control actions. The framework's performance was validated through a high-fidelity dynamic simulation of four ECs (prosumers and controllable loads) integrated into a realistic urban grid test system. When benchmarked against a standard fixed-weight particle swarm optimisation (PSO) controller, the proposed adaptive framework demonstrates significant, quantifiable contributions to both economic and environmental sustainability. Results show a 19.52% reduction in operational costs, an 8.38% decrease in power losses, and a 41.78% reduction in equivalent CO_2 emissions (improving community efficiency and environmental impact). Crucially, the framework also secured a 7.52% increase in renewable energy utilisation, directly reducing energy waste. This work proves that transitioning to intelligent, adaptive management is not merely a technical improvement but a necessity for enabling economically viable, resilient, and cleaner future energy systems.

* Corresponding author.
E-mail addresses: pablo.horrillo@uca.es (P. Horrillo-Quintero), pablo.garcia@uca.es (P. García-Triviño), javadi@fe.up.pt (M.S. Javadi), luis.fernandez@uca.es (L.M. Fernández-Ramírez), catalao@fe.up.pt (J.P.S. Catalão).

https://doi.org/10.1016/j.jclepro.2026.148033
Received 16 November 2025; Received in revised form 23 January 2026; Accepted 15 March 2026

1. Introduction

The global energy paradigm is undergoing a profound transformation, driven by international decarbonisation policies and the precipitous decline in the cost of distributed energy resources (DERs) such as photovoltaic (PV) systems and battery energy storage systems (BESS) (Chen et al., 2025). This transition is fundamentally reshaping the grid, causing the traditional, centralised model of unidirectional power flow to cede ground to a decentralised architecture built around the active "prosumer". In this new energy paradigm, ECs have evolved into core socio-technical mechanisms for managing energy at the consumer's level (Tan et al., 2025; Shi et al., 2024). As documented extensively in the literature, energy communities (ECs) provide a framework to enhance economic efficiency for their members, increase the self-consumption of renewable energy technologies (RETs), minimise power distribution losses, and integrate advanced demand side management (DSM) strategies (Sepehrzad et al., 2026).

Significant research has focused on the economic and operational optimisation of ECs (Habib, 2025), often employing sophisticated mathematical programming techniques (Yan et al., 2025). For instance, mixed-integer linear programming (MILP) has been applied to integrate energy system design with demand-side flexibility, enabling the quantification of both economic and environmental benefits for different user aggregations (Carraro et al., 2024). Similarly, second-order cone programming (SOCP) has been employed to navigate trade-offs between conflicting revenue streams, while satisfying network constraints (Siano et al.). From a metaheuristic standpoint, the genetic algorithm (GA) has been developed to address complex combinatorial problems such as optimal participant selection and energy allocation, aiming to enhance self-consumption and achieve favourable payback periods (Lazzari et al., 2023).

A common thread in these valuable approaches, however, is their reliance on simplifications to ensure computational tractability. Whether through the inherent static, scheduling nature of MILP (Carraro et al., 2024), the necessary linearisation of network constraints for SOCP (Siano et al.), or the steady-state energy balance models used with GA (Lazzari et al., 2023), these frameworks are fundamentally designed for offline planning and strategic analysis. Consequently, they inherently fail to capture the non-linear behaviours and transient dynamics critical for stability assessments, leaving a significant gap in the development of genuine dynamic control strategies. Similar papers can be found in works that address complementary challenges, such as the development of tools for fair peer-to-peer (P2P) cost allocation (Fotopoulou et al., 2025), the simultaneous optimisation of supply and demand sides (Zhang et al., 2024), and the application of robust optimisation models to manage system uncertainties (Dorahaki et al., 2025).

Regarding the DSM problem in ECs, the literature shows two dominant approaches. The first, and most common, is treating it as a direct, offline scheduling problem, which is often solved using metaheuristic algorithms. A clear example is presented in (Rollo et al., 2025), where a GA was employed to optimise day-ahead load profiles at the appliance level to enhance generation-consumption synchronisation. Ant colony and genetic algorithms (ACO-GA) were introduced to reduce community peak load and costs more effectively in (Silva et al., 2024). Even in more complex multi-energy systems, such as energy hubs, metaheuristics are used to co-optimise electrical and heating loads through scenario analysis (Zeng and Yi, 2025). An alternative approach focuses on indirect, market-based mechanisms to elicit flexibility, rather than scheduling it directly. This includes the design of price-based demand response schemes (Tan et al., 2024), where multi-stage incentive mechanisms are created to motivate prosumers to provide grid flexibility through aggregators (Ikuta and Aki, 2025). A different strategy involves creating decentralised P2P markets, often solved with the alternating direction method of multipliers (ADMM) algorithm, which enables prosumers to trade energy locally and offer their flexibility to the distribution system operator (DSO) for congestion management (Aminlou et al., 2024).

However, a crucial limitation unites both the direct scheduling and the market-based paradigms: they are fundamentally steady-state, planning-oriented frameworks. They operate on forecasted data over longer time horizons (day-ahead, hour-ahead) and inherently lack the feedback mechanisms for dynamic control. Consequently, they fail to address the critical challenges of transient stability and rapid response to unforeseen disturbances, leaving a clear research gap for treating DSM not as a planned response, but as a fully integrated, dynamically controllable resource within a closed-loop energy management system (EMS) (Yang et al., 2019).

To overcome these limitations, distributed and decentralised control architectures have gained significant traction. For example (Aittahar et al., 2023), presented an optimal control framework to co-optimise controllable assets to reduce community costs. The framework in (Zabihinia Gerdroodbari et al., 2024) empowered the distribution network service provider to manage overvoltage and line congestion by issuing dynamic export limits to prosumers. This was achieved through the collaborative management of a community energy storage system to ensure network constraints were respected. The work in (Yang et al., 2025) addressed the uncertainties of renewable generation by proposing a local energy system that integrated an electro-hydrogen coupling system with a supply-demand collaboration strategy. For its management, a two-stage stochastic optimisation model was developed. It used an extreme-scenario envelope technique, combined with response deviation coefficients, to handle supply and demand variability. However, these approaches operated on an hourly time horizon, treating the problem as a sequence of steady-state steps, without accounting for the faster, sub-hourly system dynamics.

While initial research has explored the optimisation of ECs, a notable gap in the literature remains regarding the comprehensive analysis of ECs under advanced control architectures (Kelepouris et al., 2025). The development of such frameworks points towards the hierarchical integration of distinct control paradigms. Adaptive model predictive control (AMPC) provides a rigorous methodology for predictive, multi-variable optimisation under stringent physical constraints, making it highly effective for the optimal dispatch of system assets (Wang et al., 2024). Concurrently, fuzzy logic (FL) offers a powerful approach to high-level supervisory control, capable of emulating expert heuristic reasoning to manage uncertainty and adapt strategic objectives (Dimitroulis and Alamaniotis, 2022). The synergy between AMPC's optimal control engine and FL's adaptive supervisory layer, therefore, presents a compelling pathway to address the identified research gap. A truly resilient and efficient EMS for this new era must be built upon three synergistic pillars: (i) high-fidelity dynamic modelling of RETs and energy storage systems (ESSs), (ii) adaptive intelligent power allocation, and (iii) holistic system integration. Current research on ECs, while valuable, fails to unify these aspects: steady-state models violate the first pillar, fixed-parameter controllers neglect the second, and the siloed management of generation and demand undermines the third.

This paper fills this gap by introducing a novel synergistic FL-AMPC EMS which incorporates dynamic DSM. The AMPC serves as the robust control engine for optimal power dispatch among ECs. At the same time, the supervisory FL controller functions as an expert system that processes the dynamic grid price and the concept of reserve power. This allows the framework to dynamically compute optimal weights for the AMPC, adapt its operational mode between economic and resilience-focused strategies, and simultaneously govern the flexible DSM loads as an active, closed-loop resource.

Table 1 compares current literature approaches with the paper's contribution.

The **novel contributions** of this work are articulated as follows:

1. High-fidelity dynamic EC modelling: The design and implementation of a detailed model that integrates four dynamic EC models—comprising their respective PV generators, BESS, power electronic converters, and passive and dispatchable loads—into the standard IEEE

Table 1
Comparison of the proposed control with the state-of-the-art.

Paper	Time step	Optimisation method	Dynamic control approach	DSM	BESS	Control Objective	Adaptive objectives	Hybrid strategy	Optimisation Comparison
13	15-min	Genetic algorithm	No	Yes	Yes	Cost, losses	No	No	No
14	hour	Ant colony and genetic algorithm	No	Yes	No	Cost	No	Yes	Mutated ant colony optimisation
15	hour	Modified emperor penguin colony algorithm	No	Yes	Yes	Cost, efficiency	No	No	PSO
16	hour	Carbon tracing	No	Yes	No	Cost, carbon reduction	No	No	No
17	hour	Mixed-integer linear programming	No	Yes	Yes	Cost	No	No	No
18	hour	Alternating direction method of multipliers	No	Yes	Yes	Peer-to-peer market participation	No	No	No
19	min-hour	Model predictive control	Yes	Yes	Yes	Cost	No	No	No
20	15-min	Modified model predictive control	No	No	Yes	Cost	No	Yes	No
21	hour	Mixed-integer linear programming	No	No	No	Cost	No	No	No
22	hour	Stochastic	No	Yes	No	Cost, demand fulfilment	No	No	Robust
Paper	Microseconds ($50{\cdot}10^{-6}$)	Adaptive model predictive control	Yes	Yes	Yes	Cost, self-sufficiency, losses minimisation, RETs usage maximisation	Yes	Fuzzy logic and adaptive model predictive control	Fuzzy logic and PSO

15-bus distribution network. This modelling framework provides a realistic, robust testing environment for analysing dynamic operations and transient phenomena, whilst accounting for complex control architectures. Conventional steady-state analyses systematically overlook this critical aspect.

2. Fuzzy logic intelligent supervisory controller: The design of a novel, unified control architecture that holistically coordinates generation, dispatch and DSM, addressing the limitations of both fixed-parameter and traditional siloed strategies. This is achieved through a single, intelligent supervisory control layer utilising FL. Driven by high-level grid indicators (dynamic energy price and reserve power), the FL system simultaneously executes two pivotal functions: it computes a continuous, dynamic set of optimal weights for the underlying multi-objective AMPC to align generation priorities with the operational context, and it determines the dynamic power setpoint for flexible loads. This dual-output structure ensures accurate synergistic operation, transforming DSM from a passive, scheduled resource into an active, closed-loop control variable managed in concert with generation.
3. Adaptive model predictive control strategy: The implementation and validation of an intelligent AMPC capable of autonomously transitioning the network's operational state between two distinct modes. Driven by the outputs of the FL supervisor, the system can operate in a ‘Cost-Minimisation Mode’, which leverages grid participation when prices are favourable, or seamlessly shift to a security-focused ‘Local-Reliance Mode’, which prioritises self-sufficiency when grid prices are high or internal power reserves are low.

The remainder of this paper is organised as follows: Section 2 develops the dynamic model of the ECs. Section 3 introduces the proposed hierarchical FL-AMPC framework. Section 4 details the PSO benchmarking strategies for comparison purposes. Subsequently, Section 5 presents and discusses the simulation results. Finally, Section 6 draws the main conclusions from this work.

2. High-fidelity dynamic model of energy communities

The high-fidelity dynamic modelling framework for ECs is developed in MATLAB/Simulink. A standard IEEE 15-bus distribution network is selected as the test framework, serving as a well-documented testbed. The network's architecture consists of four distinct ECs connected at different buses, which comprises a series of distributed passive loads, and a set of dispatchable loads designed to enable DSM. The overall topology of the ECs is depicted in Fig. 1a.

The four ECs integrate RET, BESS, and passive and dispatchable loads. These are categorised into two types: two larger ECs with a total rated capacity of 440 kW (a 240 kW PV plant and a 200 kW BESS), and two smaller ECs with a total rated capacity of 380 kW (a 180 kW PV plant and a 200 kW BESS). Internally, each EC's PV and BESS units are connected to a common DC bus. The PV array's operation is governed by a DC/DC converter that employs a maximum power point tracking (MPPT) algorithm to maximise energy extraction from available solar irradiance.

The interface between each EC and the central AC grid is managed by a three-phase DC/AC voltage source inverter. This converter operates in a grid-following control mode, regulating the active and reactive power injected into the community. A phase-locked loop (PLL) ensures synchronisation with the grid. At the same time, a conventional pulse-width modulation (PWM) scheme generates the switching signals. To ensure high power quality, an RLC filter is installed at the converter's output to mitigate switching harmonics. A step-up transformer then elevates the voltage from the 0.48 kV EC level to the 11 kV level of the distribution network. The transmission lines within the network are represented by their equivalent RL series impedance, and the utility grid is modelled as a real three-phase voltage source. A detailed schematic of the individual EC structure is shown in Fig. 1b. The standard single-diode model equation describes the non-linear current-voltage characteristic of the PV generation:

$$I_{PV} = I_{ph} - I_o \left[e^{\left(\frac{V_{PV} + I_{PV} R_s}{n V_T} \right)} - 1 \right] - \frac{V_{PV} + I_{PV} R_s}{R_{sh}} \tag{1}$$

where I_{PV} and V_{PV} are the PV panel's terminal current and voltage, respectively; I_{ph} is the photocurrent generated, which is directly proportional to solar irradiance; I_o represents the diode's reverse saturation current; and R_s and R_{sh} are the series and shunt resistances of the equivalent circuit.

The BESS's dynamic behaviour is implemented using a standard model from the Simscape Electrical™ toolbox. The model's dynamics,

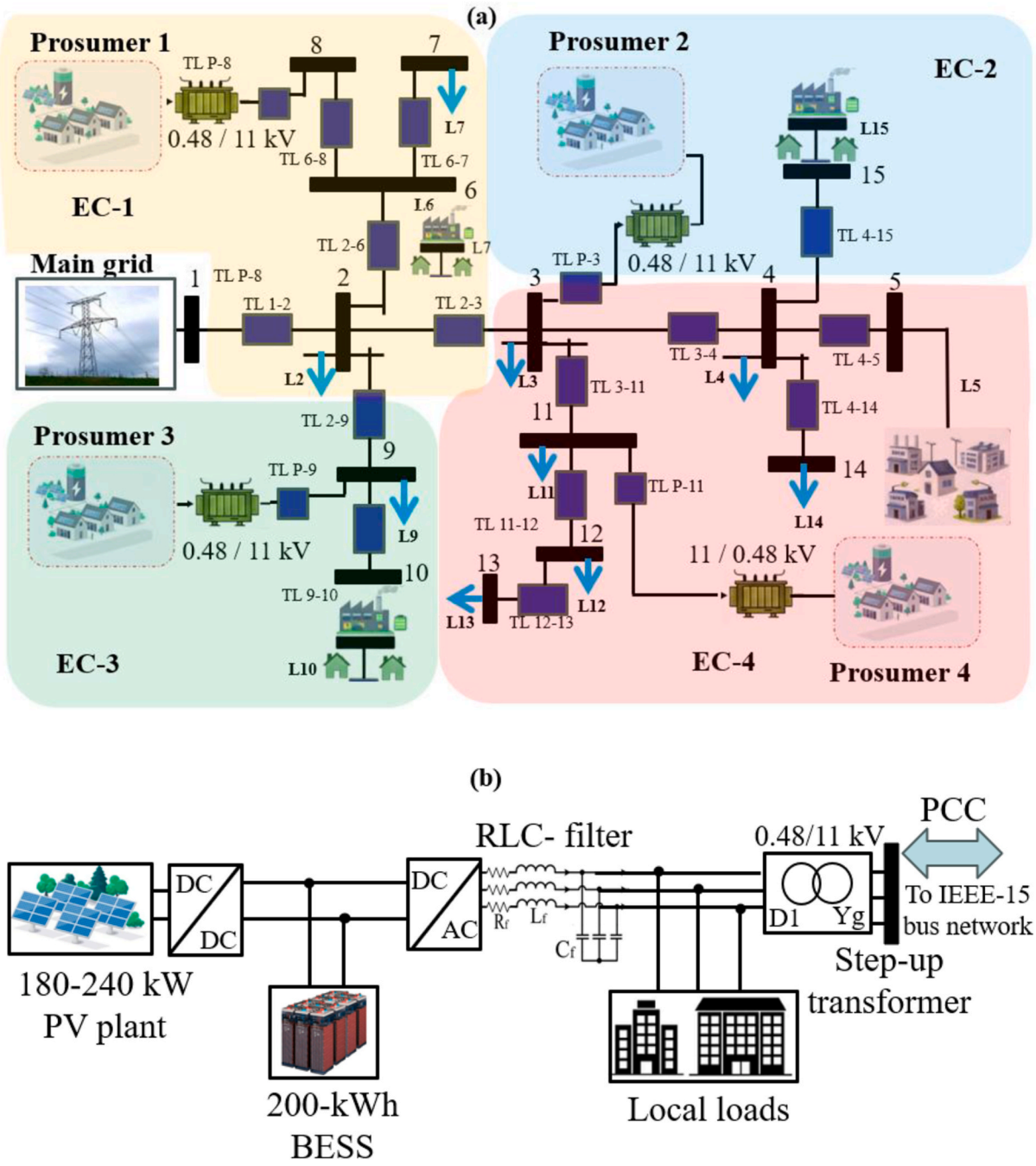

Fig. 1. Configuration of the prosumer-based EC: (a) IEEE-15 bus network ECs and (b) prosumer architecture.

particularly the terminal voltage (V_{BESS}) and the State of Charge (SOC), are governed by the following equations, which account for the open-circuit voltage (E_{BESS}) and BESS current (I_{BESS}), internal resistance (R_{int}), and nominal capacity (Q_{BESS}):

$$V_{BESS} = E_{BESS} - I_{BESS} \cdot R_{int} \tag{2}$$

$$SOC(\%) = SOC_O(\%) - 100\left(\frac{\int I_{BESS}.dt}{Q_{BESS}}\right) \tag{3}$$

3. Integrated FL-AMPC energy management system

This section details the design and operation of the proposed integrated FL-AMPC EMS. The architecture is built upon a two-layer control structure designed to synergise high-level intelligent decision-making with low-level optimal control.

Fig. 2 illustrates the integrated FL-AMPC EMS scheme. The designed EMS is architected as a hierarchical framework comprising two distinct yet synergetic control layers. At the apex, the hierarchy features a high-level FL supervisory layer, which provides strategic guidance to the underlying AMPC power dispatch layer.

The top layer acts as the system's strategic core, receiving two critical dynamic inputs from the IEEE-15 bus network: the aggregated available power ($\sum_{i=1}^{n} P_i^{ava}$) and the primary grid energy price (C_{GRID}). The FIS processes these two inputs to generate a strategic command vector consisting of five distinct outputs. These include the setpoint for the manageable loads (P_{DSM}), which operationalises the DSM strategy, and four adaptive weights ($w_{LOAD,k}$; $w_{COST,k}$, $w_{LOSS,k}$, $w_{U,k}$). The variable $w_{LOAD,k}$ represents the weighting factor assigned to the self-sufficiency

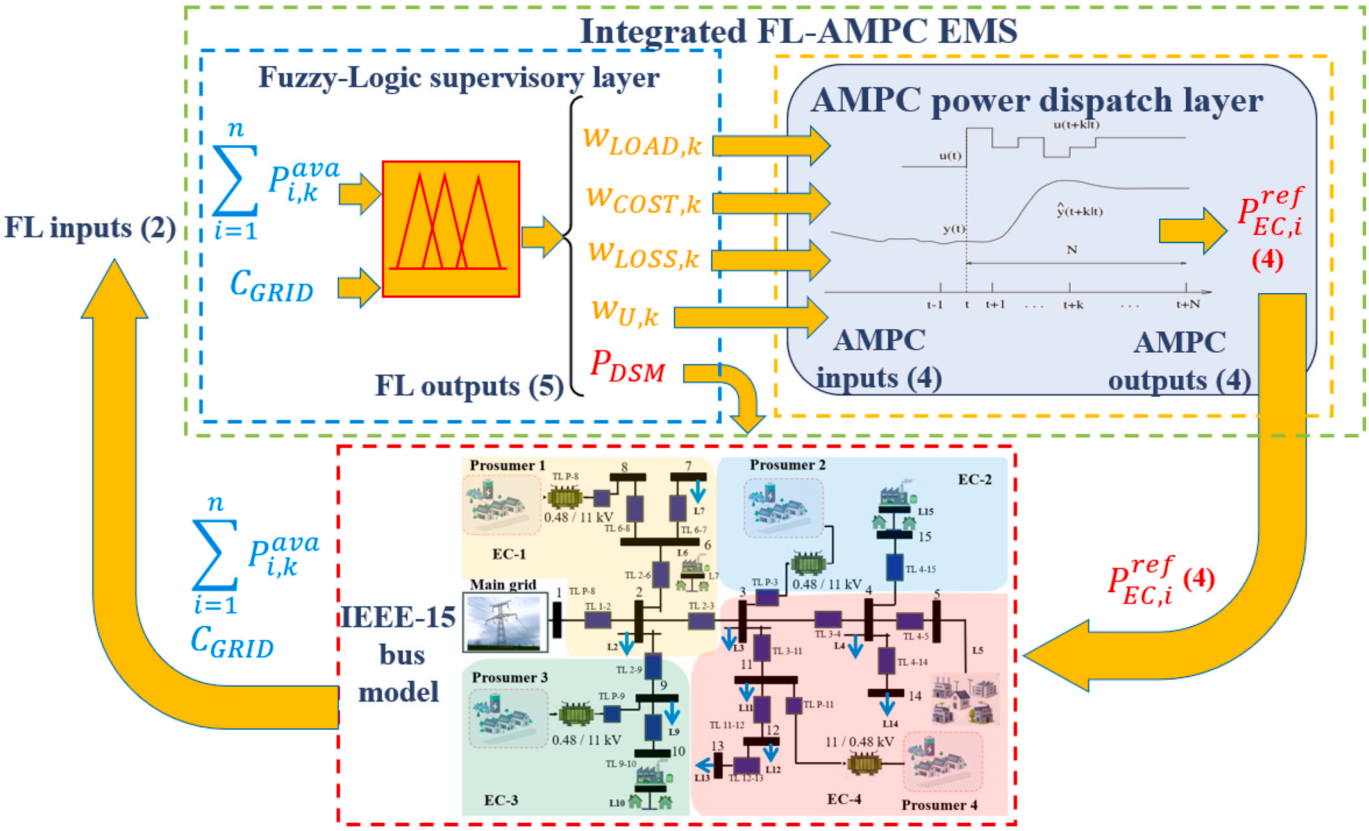

Fig. 2. Integrated FL-AMPC architecture.

control objective. $w_{COST,k}$ defines the weight for cost optimisation. Similarly, $w_{LOSS,k}$ signifies the weighting factor for power loss minimisation, and finally, $w_{U,k}$ corresponds to the control objective governing the utilisation of RETs.

A key aspect of this integrated architecture is the coupling between layers: the four adaptive weights produced by the FIS serve as the primary inputs for the lower layer. The second level, or optimal control layer, consists of an AMPC engine that utilises these four weighting inputs to guide its multi-objective optimisation process. Consequently, the AMPC layer generates four precise output references ($P_{EC,i}^{ref}$), which dictate the optimal power dispatch for each one of the four ECs. This structured exchange of variables ensures seamless integration, with the high-level heuristic reasoning of the FL layer directly modulating the deterministic optimisation of the AMPC, effectively closing the control loop within the IEEE-15 bus network.

At each time step, the controller's cost function seeks to satisfy four distinct goals concurrently:

(i) Enhance the IEEE-15 bus distribution network self-sufficiency by maximising the use of ECs to meet demand.
(ii) Reduce the overall operating expenditures considering the ECs and the grid participation.
(iii) Improve technical efficiency by minimising power losses during generation.
(iv) Promote the self-consumption of renewable energy by maximising its integration.

The controller's adaptive nature enables it to adjust the relative importance of these objectives autonomously. The cost function weights are continuously modulated by the external electricity market price signal, allowing the system to intelligently shift its operational strategy between modes, such as prioritising cost reduction or local resilience.

3.1. Fuzzy logic intelligent supervisory controller

The top-level intelligent controller within the hierarchical EMS is the FL supervisory controller. The fundamental challenge in managing several ECs lies in navigating the complex, non-linear, and often conflicting trade-offs between economic performance and operational resilience, i.e., a task for which traditional, model-based controllers are ill-suited. A Mamdani Type-2 fuzzy inference system (FIS) is therefore selected as the ideal architecture, as its intuitive, linguistic rule-based structure allows direct encoding of expert knowledge. Its defuzzification process produces a continuous, smooth control surface, ensuring stable command signals (Vidal-Martínez et al., 2025).

The architecture of the designed FIS is defined by its interface with the system: two critical inputs and five strategic outputs. The inputs are carefully selected to provide the controller with a concise yet comprehensive snapshot of the system's dynamic operational context. To provide a clear operational framework, a distinction is established between the passive loads ($P_{PASSIVE}$), which represent the non-controllable baseline demand, and the active loads subject to DSM (P_{DSM}), which constitute the manageable demand segment. The first, reserve power (P_{RES}), quantifies the community's physical capacity and resilience. It can be defined as:

$$P_{RES,k} = \sum_{i=1}^{n} P_{i,k}^{ava} - \sum P_{PASSIVE,k} \tag{4}$$

$P_{RES,k}$ denotes the instantaneous power availability in the IEEE 15-bus network to accommodate manageable demand after the passive consumption requirements have been met. The reserve power is derived as the net difference between the aggregated available power ($P_{i,k}^{ava}$) and the aggregated passive demand ($P_{PASSIVE,k}$), effectively representing the energy margin available to satisfy the demand of the controllable DSM loads.

The concept of available power is defined as:

$$P_i^{ava} = P_{PV,i} + P_{BESS,i} - P_{P,LOAD,i} \quad (5)$$

It details the dynamic capacity inherent to each EC. This formulation integrates the power injected by the PV power plant ($P_{PV,i}$) and the BESS ($P_{BESS,i}$), while subtracting the internal prosumer demand ($P_{P,LOAD,i}$). Consequently, the available capacity within each EC to supply the diverse nodes of the IEEE 15-bus network constitutes a comprehensive global computation of the local generation potential and the internal requirements of the prosumers. This hierarchical approach ensures that the supervisory layer operates with a precise understanding of the net energy balance before initiating demand-side interventions.

P_{RES} is represented by five linguistic membership functions (very low, low, medium, high, very high). The second input, primary grid price (C_{GRID}), captures the grid economic dynamic conditions, described by three membership functions (low, medium, high). Based on these two inputs, the FL controller simultaneously generates five distinct outputs that form a complete strategic command vector: four adaptive weights for the AMPC's multi-objective function at each sample time (k) ($w_{LOAD,k}$; $w_{COST,k}$, $w_{LOSS,k}$, $w_{U,k}$) and a direct power setpoint for the DSM loads ($P_{DSM,k}$). This latter output functions as an active control signal that determines the magnitude of demand to be managed at each interval. By adjusting this setpoint within a regulated range of 0 to 400 kW, the FIS dynamically modulates the flexible demand to mitigate peak loads or leverage surplus generation, effectively serving as a primary instrument for system stability.

Furthermore, the total electrical demand of the IEEE-15 bus network (P_{LOAD}^{TOT}) is explicitly defined as the aggregate of both non-controllable and controllable components:

$$P_{LOAD}^{TOT} = P_{PASSIVE} + P_{DSM} \quad (6)$$

The specific shapes and ranges of these membership functions, which define the linguistic variables, are detailed in Fig. 3.

The control philosophy of the supervisory layer is encoded in a linguistic rule base, which constitutes the system's expert knowledge base. The rules shown in Table 2 dictate the strategic posture of the entire network, positioning the DSM load as a critical flexibility instrument for dynamic balancing. For instance, during periods of high reserve power and high grid prices, the strategy shifts to avoid primary grid consumption by promoting local energy utilisation. In this scenario, the FL controller assigns a high priority to the self-sufficiency weight ($w_{LOAD,k}$) while decisively reducing the cost weight ($w_{COST,k}$). Simultaneously, it issues a high value for P_{DSM}, effectively acting as a 'valley-filling' mechanism that absorbs surplus internal generation to prevent inefficient exports to the grid at low compensation rates.

Conversely, when reserve power is very low, and the grid price is low, the strategy is inverted to prioritise economic opportunism by

Table 2
Fuzzy logic rules.

INPUTS		OUTPUTS				
P_{RES}	C_{GRID}	w_{LOAD}	w_{COST}	w_{LOSS}	w_{USE}	P_{DSM}
VL	L	L	H	H	L	L
VL	M	L	H	N	L	L
VL	H	L	L	H	L	L
L	L	L	H	H	L	L
L	M	N	N	N	L	L
L	H	L	L	H	L	L
M	L	L	H	H	H	M
M	M	N	N	N	M	M
M	H	H	L	H	M	M
H	L	L	H	H	H	H
H	M	N	N	N	H	H
H	H	H	L	H	H	H
VH	L	L	H	H	H	H
VH	N	N	N	N	H	H
VH	H	H	L	H	H	H

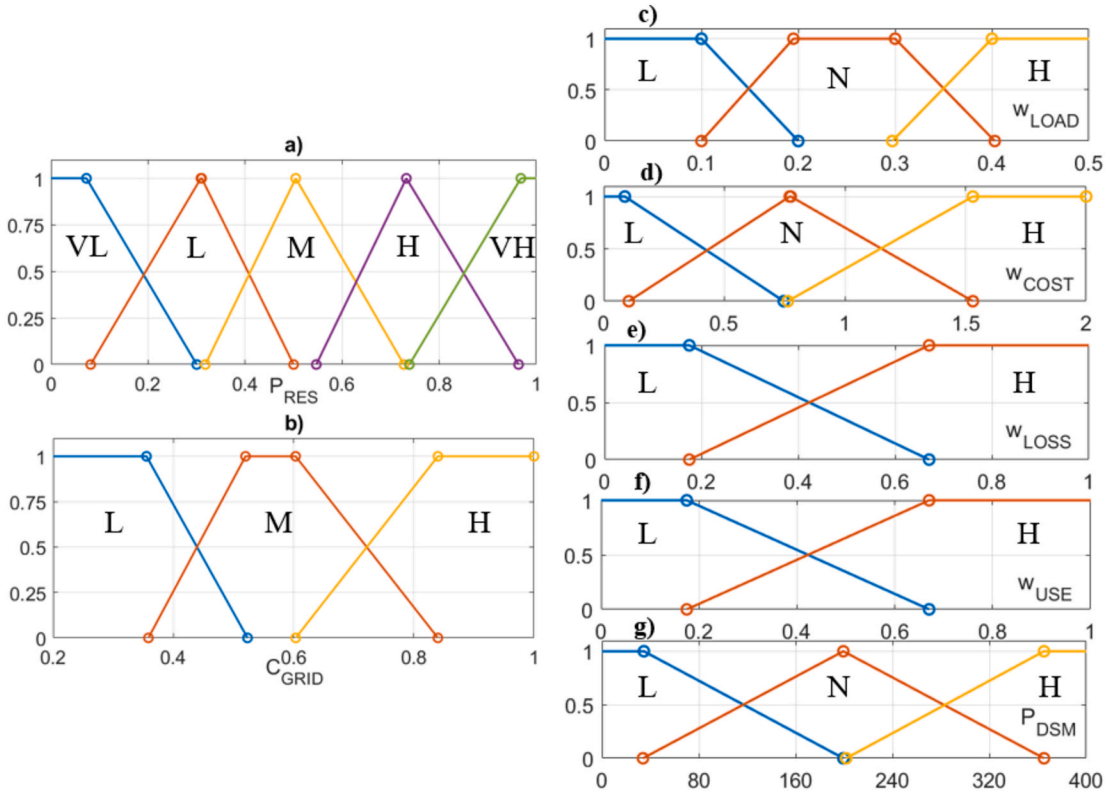

Fig. 3. Fuzzy logic membership functions: (a) P_{RES}, (b) C_{GRID}, (c) w_{LOAD}, (d) w_{COST} (e) w_{LOSS}, (f) w_{USE} and (g) P_{DSM}

maximising the cost weight ($w_{COST,k}$) to allow for strategic grid purchases. In this context, the FIS commands a low value for P_{DSM}, performing a demand-curtailment action to preserve scarce internal resources for essential passive loads. This dual-action role, shifting consumption to periods of high availability and shedding non-critical demand during scarcity, allows the DSM framework to enhance the overall resilience and economic efficiency of the 4-EC cluster. Given that minimising generation losses and maximising the utilisation of RETs are concurrently desirable objectives, their respective weights are assigned a balanced distribution across all operational modes.

The crucial link between the supervisory FL and AMPC optimal power dispatch layer is the dynamic weight adjustment mechanism. The central contribution of this work lies in the intelligent, dynamic arbitration of the AMPC's control objectives, guided by the adaptive weight vector. Unlike conventional MPC with static priorities, which is locked into a perpetual, suboptimal compromise, the proposed framework employs a state-aware supervisory logic that dynamically reconfigures the controller's definition of 'smart'. This allows the system to explicitly manage the inherent trade-offs between conflicting goals, a critical capability for the robust operation of the EC. This adaptation dictates the transition between two distinct extreme operational philosophies:

- Resilience-oriented: During periods when the grid price is high, purchasing external energy becomes either economically prohibitive or physically risky. In this scenario, the FL supervisor activates a resilience-focused strategy. It assigns a dominant priority to $w_{LOAD,k}$, while significantly reducing the importance of $w_{COST,k}$. The AMPC's overriding goal is to operate the ECs as an autonomous, efficient entity, minimising power imports from the primary grid. This strategy ensures security of supply by maximising the utilisation of local assets, potentially offering lower internal operating costs than a grid-dependent approach.
- Economic-oriented: Conversely, when market conditions are favourable (low grid price), the system's operational mode is inverted to engage an economic optimisation strategy. The priorities shift decisively, and $w_{COST,k}$ is given dominant importance. The AMPC then seeks the most economically efficient power dispatch, typically resulting in a hybrid solution in which the cheapest local resources cover part of the demand and are also imported opportunistically from the low-cost grid. The accepted consequence of this economically driven strategy is a reduction in the community's self-consumption of its own renewable assets in favour of immediate financial benefit.

It is crucial to note that the FL controller does not simply switch between these two binary states. Instead, it continuously and smoothly modulates the entire set of four weights, creating a spectrum of hybrid strategies. A conventional fixed-weight MPC is rendered suboptimal the moment external conditions change; during low-price periods, it fails to capture economic surplus, while during high-price periods, it bleeds value by failing to enforce self-sufficiency. However, the proposed framework transcends this fundamental limitation. By dynamically reshaping the cost function's topology, the FL supervisor actively steers the optimiser towards the most advantageous solution that aligns with the current operational context, marking a paradigm shift from a fixed, compromise-based methodology to a dynamic, brilliant control strategy.

Finally, it is noteworthy that the proposed control architecture, by relying on universal and technologically neutral power metrics such as P_{ava} and P_{RES} is inherently scalable to more complex energy paradigms. This modularity enables seamless integration of multi-energy assets, such as thermal loads served by electric or gas-fired boilers. Within this expanded framework, the FIS would dynamically orchestrate these units by prioritising electric-to-thermal conversion during periods of abundant renewable surplus or favourable grid pricing, whilst strategically pivoting to gas-fired production during energy scarcity to preserve electrical resources. Furthermore, the framework is designed to accommodate other types of ESSs. For instance, the integration of hydrogen-based technologies illustrates this versatility; fuel cells would directly contribute to the P_{ava} computation by leveraging green hydrogen produced via surplus photovoltaic generation. Simultaneously, electrolysers would be managed as high-capacity ESSs operating in tandem with electrical batteries, thereby significantly extending the operational flexibility and resilience of the ECs. Consequently, the EMS provides a robust and future-proof solution that maintains its competitiveness and operational integrity across a broad spectrum of energy assets.

3.2. Adaptive model predictive control formulation

Within the hierarchical framework, the AMPC serves as the optimal control engine, operating under the receding-horizon principle. Fig. 4 presents the AMPC blocks diagram. At each sampling instant, the AMPC leverages a dynamic model of the ECs to predict the system's future behaviour over a defined prediction horizon (N_P). Based on this prediction, it solves a constrained, finite-horizon optimisation problem to compute an optimal sequence of future control actions, i.e., the power dispatch setpoints over a control horizon (N_C) (Ramirez-Marin et al., 2025). This optimisation minimises a multi-objective cost function whose priorities are dictated by the adaptive weights from the FL supervisor. The system state shifts forward, the horizon extends, and the entire predict-and-optimise process is repeated, ensuring continuous feedback and robust control. A set of control inputs and system outputs defines the AMPC. The control input vector, (u_k), comprises the manipulated variables (MVs), which are the active power setpoints for each prosumer at each discrete time step k. This vector is defined as:

$$u_k = \begin{pmatrix} P^{ref}_{EC,1} \\ P^{ref}_{EC,2} \\ P^{ref}_{EC,3} \\ P^{ref}_{EC,4} \end{pmatrix} \tag{7}$$

The AMPC's optimisation algorithm computes these setpoints by employing a quadratic programming solver based on predictions of the ECs' operating states, including passive and dispatchable demand, renewable energy availability, SOC state, and grid electricity prices.

The system output vector captures the system's response to these inputs, y_k, which is composed of four key performance indicators (KPIs): the total power dispatched by the prosumers ($P_{TOT,k}$), the total instantaneous operating cost ($C_{TOT,k}$), the total power losses ($L_{TOT,k}$), and a renewable energy utilisation index ($U_{RET,k}$). This vector is expressed as:

$$y_k = \begin{pmatrix} P_{TOT,k} \\ C_{TOT,k} \\ L_{TOT,k} \\ U_{RET,k} \end{pmatrix} \tag{8}$$

The total dispatched power is computed as:

$$P_{TOT,k} = \sum_{i=1}^{n} P_{i,k} \tag{9}$$

where P_i denotes the power of each EC.

The total cost ($C^{tot}_{op,k}$) aggregates the individual generation costs of each EC ($C_{i,k}$), the cost of power imported from the primary grid ($P_{GRID,k}$ at cost $C_{GRID,k}$), and the cost attributed to power losses ($P_{L,k}$ at cost $C_{L,k}$):

$$C_{TOT,k} = \sum_{i=1}^{n} P_{i,k} \cdot C_{i,k} + P_{GRID,k} \cdot C_{GRID,k} + P_{L,k} \cdot C_{L,k} \tag{10}$$

The total power losses ($P_{L,k}$) are modelled as a quadratic function of the currents flowing from each EC ($I_{i,k}$) and the grid ($I_{GRID,k}$), considering

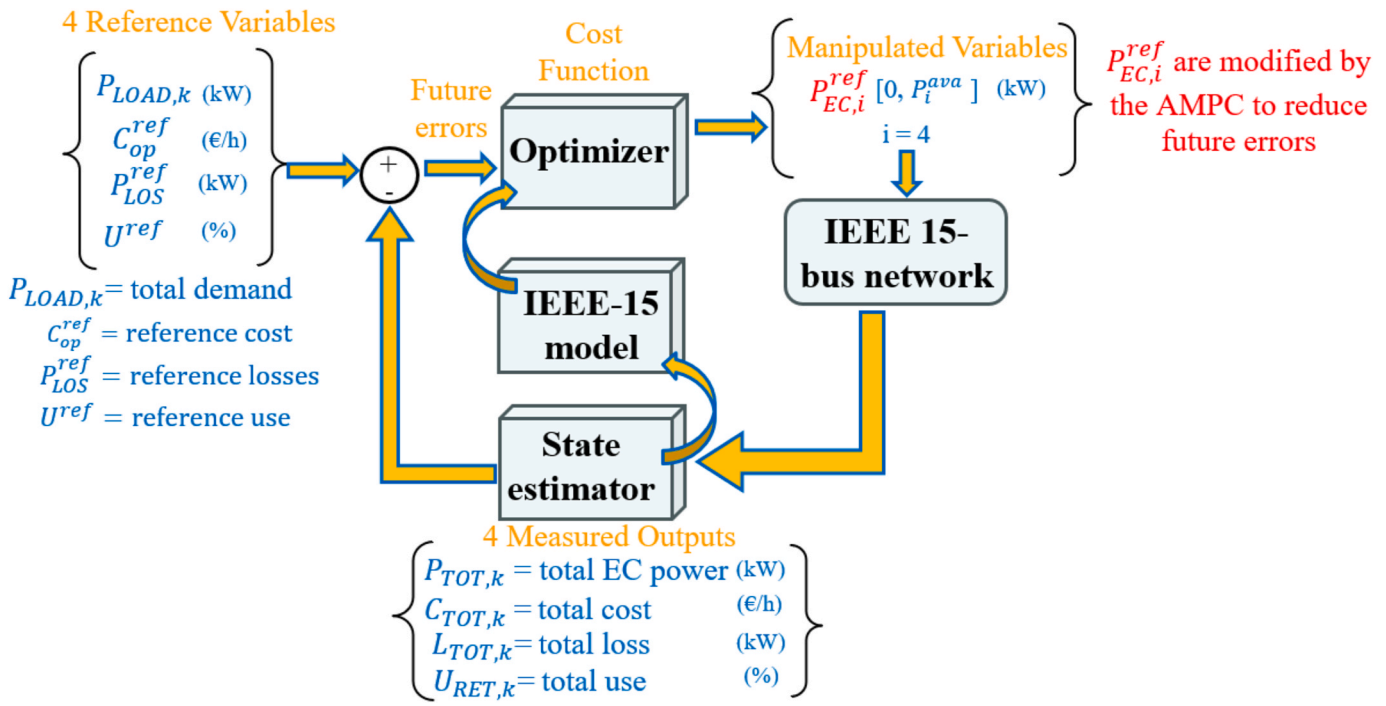

Fig. 4. Adaptive model predictive control architecture.

their respective equivalent resistances (R_i, R_{GRID}):

$$L_{TOT,k} = \sum_{i=1}^{n} 3 \cdot \left(R_i \cdot I_{i,k}^2\right) + 3 \cdot \left(R_{GRID} \cdot I_{GRID,k}^2\right) \tag{11}$$

Finally, the RET utilisation index ($U_{RET,k}$), measures the effective use of the total available capacity of the ECs:

$$U_{RET,k} = \sum_{i=1}^{N} \frac{P_{i,k} \cdot P_{i,k}^{ava}}{\left(P_{i,k}^{ava}\right)^2} \tag{12}$$

Regarding the optimisation problem, the main goal is to compute an optimal sequence of future control actions, $\Delta U\,(k)$, over a defined control horizon (N_C) that minimises a comprehensive cost function, within a longer prediction horizon (N_P). The cost function is formulated as a weighted sum of predicted future errors:

$$\min(J) = \sum_{i=1}^{N_P} [y(k+i|k) - w(k+i|k)]^2 \lambda_1 + \sum_{i=1}^{N_C} [\Delta u(k+i-1|k)]^2 \lambda_2 \tag{13}$$

The objective function J serves as the mathematical core of the AMPC power dispatch layer, balancing multi-objective performance with operational stability via a quadratic optimisation approach. The first summand, defined as the tracking or error term, calculates the squared difference between the predicted system outputs $y(k+i|k)$ and the desired reference trajectories or setpoints $(k+i|k)$ over the prediction horizon N_P. This term ensures that the ECs adhere to their target performance metrics, such as self-sufficiency, cost reduction, loss minimisation or RETs utilisation, weighted by the dynamic factor. w_1, which is directly informed by the adaptive outputs of the FL supervisory layer.

Complementing this, the second summand represents the control effort or move suppression term, which penalises the magnitude of the incremental control actions $\Delta u(k+i-1|k)$ over the control horizon N_C by actuating in the control actions or manipulated variables, thus, the power references of each EC $\left(P_{EC,i}^{ref}\right)$. By weighting these control increments with λ_1, the controller effectively prevents aggressive or oscillatory variations in $P_{EC,i}^{ref}$. This predictive foresight enables the AMPC to proactively manage future grid variations while ensuring stable and gradual transitions. Essentially, it transforms the high-level strategic objectives into precise, actionable power references for the IEEE-15 bus network.

The reference vector, $r(k)$, is defined to guide the optimisation towards ideal performance:

$$r_k = \begin{pmatrix} P_{LOAD,k} \\ 0 \\ 0 \\ 1 \end{pmatrix} \tag{14}$$

The reference power of the ECs is the total system demand $P_{LOAD,k}$, which is obtained as the sum of $P_{PASSIVE}$ and P_{DSM}. The cost and loss references are set to zero, and the utilisation reference is set to one. Although these three setpoints are physically unattainable due to the operation and the constraints established, they allow for the search for an optimal solution.

To conduct a feasible operation, the optimisation is therefore performed within several operational constraints. The fundamental power balance constraint that must be satisfied at every time step is defined as:

$$\sum_{i=1}^{N} P_{i,k} + P_{GRID,k} = P_{LOAD,k} + L_{TOT,k} \tag{15}$$

Moreover, the inclusion of dynamic constraints provides a high-level adaptive problem formulation and adaptive weighting. To this end, the power delivered by each EC is dynamically constrained by its available capacity, which depends on irradiance and BESS SOC.

$$P_{i,k} \leq P_{i,k}^{ava} \tag{16}$$

The BESS SOC is dynamically constrained between an upper and lower threshold (Horrillo-Quintero et al., 2025):

$$P_{BESS,dis}^{max} = min\left(P_{BESS}^{rated}, \frac{E_{BESS}^{nom}}{\Delta t} \cdot \left(\frac{SOC - SOC_{min}}{100}\right)\right) \tag{17}$$

$$P_{BESS,ch}^{max} = min\left(P_{BESS}^{rated}, \frac{E_{BESS}^{nom}}{\Delta t} \cdot \left(\frac{SOC_{max} - SOC}{100}\right)\right) \tag{18}$$

In these constraints, $P_{BESS,dis}^{max}$ and $P_{BESS,ch}^{max}$ represent the maximum

allowable discharging and charging power rates, respectively, while P_{BESS}^{rated} is the battery's nominal power. The term $\frac{E_{BESS}^{nom}}{\Delta t}$ corresponds to the instantaneous rate of change of energy. Finally, SOC_{min} and SOC_{max} define the lower and upper operational bounds for the BESS SOC. The AMPC parameters are detailed in Table 3.

The parameters detailed in Table 2 were selected through a careful tuning process to ensure robust, effective control performance, based on the recommendations of (Vivas et al., 2025). The prediction horizon (N_P) was chosen to be sufficiently long to capture the key short-term dynamics of the system, such as fluctuations in renewable generation and electricity prices, enabling anticipatory control actions. The shorter control horizon (N_C) represents a deliberate trade-off that reduces the dimensionality of the optimisation problem to ensure computational tractability within the sampling time. The ranges for the objective function weights were normalised to reflect the underlying control philosophy, providing the FL supervisor with sufficient leverage to dynamically prioritise economic efficiency or operational resilience as the system's context evolves. Collectively, this parameter set establishes a well-balanced compromise between proactive control performance, stability, and dynamic computational feasibility.

The distinct ranges for each weight are a deliberate design choice, normalised asymmetrically to reflect a pre-defined hierarchy of control priorities. A wider range of [0, 2] was assigned to the cost weight ($w_{COST,k}$) to allow it to act as a dominant factor, enabling the controller to pursue economic optimisation aggressively. The weights for loss minimisation ($w_{LOSS,k}$) and renewable utilisation ($w_{U,k}$) were normalised to a standard range of [0, 1], establishing them as significant secondary objectives focused on technical efficiency. Finally, the weight for tracking the total power demand ($w_{LOAD,k}$) was given a narrower range of [0, 0.5]. This is because the power balance is enforced as a hard constraint; this lower-magnitude weight serves as a soft guide for the optimiser.

4. Multi-objective particle swarm optimisation benchmark

A pivotal aspect of validating any novel control architecture is its performance assessment against a credible and fundamentally different baseline. To isolate and quantify the specific benefits of predictive, horizon-based optimisation of the FL-AMPC, a non-predictive, reactive benchmark controller was designed. For this purpose, PSO was selected. As a powerful metaheuristic, PSO is adept at finding optimal solutions under current conditions without foresight or model-based prediction, making it an ideal scientific counterpart for evaluating the tangible advantages of the AMPC's predictive methodology (Li et al., 2020).

To create a scientifically rigorous benchmark, the controller's architecture was intentionally designed to be decoupled, fundamentally separating the strategic decision-making processes. In this scheme, the FL supervisor's role is strictly confined to managing DSM loads, leaving the PSO algorithm with a singular, well-defined task: solving the optimal generation dispatch problem. At each time step, it solves a multi-variable optimisation problem, finding the mathematically perfect solution within a dynamic framework. Its objective is to find the power setpoint vector, $= [P_{EC,1,k}^{ref}, P_{EC,2,k}^{ref}, [P_{EC,3,k}^{ref}, [P_{EC,4,k}^{ref}]$, that minimises a multi-variable aggregated fitness function, F. However, in stark contrast to the primary controller, this benchmark operates with a set of fixed, static weights. These weights are pre-defined to represent a balanced, "one-size-fits-all" compromise strategy. To ensure each objective has a comparable influence on the fitness function despite its different units and scales, the performance metrics were first normalised to a standard range. After this normalisation, each objective was assigned an equal weight of 0.25, reflecting a strategy in which all goals are given equal priority.

The fitness function is defined as:

$$F(u(k) = w_{LOAD} \cdot e_P(k) + w_{COST} \cdot C_{TOT}(k) + w_{LOSS} \cdot L_{TOT}(k) - w_{USE} \cdot U_{RET}(k) \quad (19)$$

where the term $e_P(k)$ denotes the error when generation does not match demand, ensuring power balance.

Table 4 details the pseudocode for the multi-objective PSO algorithm.

5. Results and discussion

This section presents a comparative analysis of the proposed FL-AMPC framework against the FL-PSO benchmark described in Section 4. To demonstrate the effectiveness and operational validity of the FL-AMPC, a rigorous comparative analysis is conducted within a high-fidelity dynamic simulation environment. A distinctive feature of this study is the adoption of a microsecond-scale simulation time step, employing 50 μs. This high level of resolution is essential, as it enables the explicit capture of fast electromagnetic transients. These phenomena are frequently neglected in conventional economic dispatch studies, yet are vital for assessing system stability and the dynamic impact of control actions involving power electronics.

The analysis is organised into four specialised subsections to provide a comprehensive and intuitive assessment of the controller's performance. Section 5.1 establishes the environmental boundary conditions

Table 3
AMPC parameters.

Item	Parameter	Value
Controller parameters	T_s Sample time (s)	10^{-2}
	N_P Prediction horizon (s)	100
	N_C Control horizon (s)	10
Constraints manipulated variables	$P_{EC,1}^{ref}$ (kW)	$[0, P_1^{ava}]$
	$P_{EC,2}^{ref}$ (kW)	$[0, P_2^{ava}]$
	$P_{EC,3}^{ref}$ (kW)	$[0, P_3^{ava}]$
	$P_{EC,4}^{ref}$ (kW)	$[0, P_4^{ava}]$
Constraints measured outputs	P_{LOAD}^{tot} (kW)	-
	C (€/h)	$[0, \infty]$
	P_{loss}^{tot} (kW)	$[0, \infty]$
	U_f (%)	[0, 1]
Weights measured outputs	$P_{P,k}^{tot}$ (kW)	[0, 0.5]
	C (€/h)	[0, 2]
	P_{loss}^{tot} (kW)	[0, 1]
	U_f (%)	[0, 1]

Table 4
Particle swarm optimisation pseudocode.

Step	Procedure
1 – Objective	The main objective is to minimise the fitness function $F(u(k))$ as defined in Eq. (19)
2 – Decision variables	The particle's position vector is defined as the power setpoints $x = [P_{EC,1,k}^{ref}, P_{EC,2,k}^{ref}, P_{EC,3,k}^{ref}, P_{EC,4,k}^{ref}]$ subject to $P_{i,k} \leq P_{i,k}^{ava}$
3 – Initialisation	Initialise a swarm of N particles with random positions x_i and velocities v_i, set initial best $x_i \rightarrow p_i$ and find the initial best g.
4 – Evaluation & update	For each particle, evaluate $F(u(k))$ and update its personal best p_i. Then, identify and update the swarm's global best position, g.
5 – Dynamics update	Update each particle's velocity and position for the next iteration: $v(k+1) = w \cdot v_i + r_1 c_1 (v_i - x_i) + r_2 c_2 (g - x_i)$ $x_i(k+1) = x_i + v_i(k+1)$ In these equations, w represents the inertia weight, c_1 and c_2 are the acceleration coefficients, while r_1 and r_2 are random numbers uniformly distributed in the range (0,1).
6 – Iteration	Repeat steps 4 and 5 until the termination condition (e.g., maximum number of iterations) is met.
7 - Output	Return the final global best position, g, as the optimal solution u_{opt} (k).

and provides a direct, side-by-side comparison of local production within each EC for the PV power plant and BESS operation, between the FL-AMPC and the FL-PSO benchmark. This section also includes a comparative evaluation of available power and the power delivered for each EC. Section 5.2 examines the resulting power dispatch for both strategies, illustrating how each framework manages energy flows under high-variability conditions. To provide a numerical comparison, Section 5.3 presents a detailed quantitative study evaluating both controllers using a suite of key performance indicators (KPIs), including economic costs, system losses, RET integration, primary grid energy consumption, and CO_2 emissions. Finally, Section 5.4 provides a holistic validation by comparing the FL-AMPC results, both qualitatively and quantitatively, with similar studies in the current literature.

The analysis is based on the IEEE 15-bus network presented in Fig. 1, with its operational parameters detailed in Table 5. The operation is driven by dynamic profiles for solar irradiance and grid prices, and by a composite load profile comprising both passive demand and loads actively managed under a DSM scheme. Crucially, the controller's performance was verified under extreme, challenging operational conditions, characterised by volatile price fluctuations and abrupt shifts in renewable generation. These high-stress conditions serve as a stringent test of the controller's core intelligent function: its ability to adaptively determine when to leverage the primary grid for economic advantage and when to incrementally increase self-sufficiency for enhanced resilience, thereby demonstrating its capacity to select the optimal operational mode under demanding conditions.

5.1. Comparative operational dynamics and delivered power profiles

Fig. 5 presents the dynamic input profiles employed for a 300-s simulation. Fig. 5(a)–5(d) delineate the four distinct solar irradiance profiles for ECs one to four, respectively, while Fig. 5e depicts the dynamic primary grid price. Throughout this analysis, the subscript i denotes variables corresponding to each EC. These profiles were selected to encompass a broad spectrum of operational exigencies. Specifically, the irradiation for the PV power plant in EC one (Irr_1) and two (Irr_2) exhibit marked oscillatory behaviour characterised by successive local maxima, fluctuating within the 600–950 W/m^2 range. Conversely, the irradiation for the PV power plant in EC three (Irr_3) follows a smooth, ramp-up and ramp-down trajectory (500–960 W/m^2), whereas for the fourth EC (Irr_4) displays a pronounced sigmoidal trend, recovering from an initial dip of 220 W/m^2 to reach a sustained upward plateau of 850 W/m^2. Collectively, these heterogeneous profiles provide a rigorous testbed for validating the controller's efficacy under conditions of substantial operational variability.

Table 5
EC parameters.

Symbol	Parameter	Unit
V_{nom}	Rated voltage	11 kV
f_{nom}	Rated frequency	60 Hz
L_{1-2}	Line parameters per phase	1.351 Ω + 3.517 mH
L_{2-3}	Line parameters per phase	1.1702 Ω + 3.036 mH
L_{2-6}	Line parameters per phase	2.557 Ω + 4.575 mH
L_{2-9}	Line parameters per phase	2.013 Ω + 3.602 mH
L_{3-4}	Line parameters per phase	0.841 Ω + 2.182 mH
L_{3-11}	Line parameters per phase	1.796 Ω + 3.213 mH
L_{4-5}	Line parameters per phase	1.532 Ω + 2.726 mH
L_{4-14}	Line parameters per phase	2.231 Ω + 3.991 mH
L_{4-15}	Line parameters per phase	1.197 Ω + 2.142 mH
L_{6-7}	Line parameters per phase	1.088 Ω + 1.947 mH
L_{6-8}	Line parameters per phase	1.251 Ω + 2.239 mH
L_{9-10}	Line parameters per phase	1.687 Ω + 3.018 mH
L_{11-12}	Line parameters per phase	2.448 Ω + 4.381 mH
L_{12-13}	Line parameters per phase	2.013 Ω + 3.602 mH
L_f	Filter inductance	1.08 mH
R_f	Filter resistance	1.08 mΩ
C	Filter capacitance	184 μF
m	Step-up transform voltage relationship	0.48/11 kV

The internal power management of each EC is detailed in Fig. 6. It depicts the interplay between the generated PV power ($P_{PV,i}$), the power from the BESS ($P_{BESS,i}$), and the total power delivered by the EC (P_i) to the IEEE-15 bus network. The four distinct operational profiles, corresponding to $E_{C,1}$ through $E_{C,4}$ in figures (a) through (h), respectively, establish the challenging and dynamic nature of the testbed for the FL-AMPC and the FL-PSO benchmark.

A comparative assessment of EC_1 reveals how each controller handles renewable intermittency. In Fig. 6a, the FL-AMPC manages a $P_{PV,1}$ that oscillates rapidly between 115 kW and 171 kW, peaking at t = 185 s. To maintain a robust total injection (P_1) of 260–300 kW, the AMPC-FL commands a sustained BESS discharge ($P_{BESS,1} > 0$) within a narrow band of 125–167 kW. Conversely, the FL-PSO in Fig. 6b exhibits a more rigid response, while $P_{PV,1}$ When the same fluctuating profile is followed, the BESS output is approximately constant at around 100 kW. Consequently, the resulting P_1 remains significantly lower (209–250 kW), lowering the EC's contribution during periods of high solar availability.

The performance disparity is further accentuated in EC_2, where the EC must navigate abrupt shifts in delivered power. In Fig. 6c, the FL-AMPC demonstrates high adaptive agility: during the initial phase (t < 60 s), $P_{PV,2}$ remains stable around 110 kW, while the BESS maintains a moderate discharge between 70 and 103 kW. At t = 60 s, in response to a shift in the global dispatch objective, the FL-AMPC triggers a sharp step-increase in the BESS output to 200 kW. This allows P_2 to reach and sustain a peak of 350 kW until t = 240 s, at which point the controller intelligently curtails the BESS discharge back to 66 kW as $P_{PV,2}$ begins to recede to 108 kW and P_2 is reduced to 177 kW. In stark contrast, the FL-PSO response in Fig. 6d is markedly more passive. The BESS output remains constant at 140 kW throughout the simulation, regardless of the solar ramp or the system's needs. As a result, P_2 is dictated almost entirely by the raw solar profile, peaking at only 286 kW, demonstrating a lower use of availability capacity compared to the proposed framework.

The remaining ECs, EC_3 and EC_4, demonstrate the controllers' proficiency in managing trending irradiance profiles and surplus energy through bidirectional BESS flexibility. For EC_3, $P_{PV,3}$ follows the bell-shaped trajectory established in Fig. 5c, peaking at approximately 230 kW around t = 130 s. In Fig. 6e, the FL-AMPC demonstrates precise regulatory control by switching the BESS into charging mode ($P_{BESS,3} < 0$). Specifically, at t = 60 s, the controller executes a step-increase in P_3, rising from 105 kW to 145 kW. To stabilise this output despite the rising PV ramp, the BESS absorbs the surplus, reaching a charging peak of −45 kW. As the solar resource recedes after t = 130 s, the BESS seamlessly transitions back to a discharge state, peaking at 35 kW to support the dispatch command until the final downward step at t = 240 s. In contrast, the FL-PSO benchmark (Fig. 6f) exhibits a more sluggish response; it maintains the BESS in a prolonged charging state for nearly the entire simulation, only changing to discharge operation mode after t = 180 s. This results in a P_3 trajectory that follows a smoother but less regulated trajectory, rising gradually from an initial 93 kW to a peak of 170 kW.

The results for EC_4 further underscores the FL-AMPC's superior adaptive capabilities. Driven by the rising $P_{PV,4}$ profile, which peaks at 24 kW, the controller must balance high-power injection requirements with surplus storage. As shown in Fig. 6g, the FL-AMPC initially commands a high discharge rate for $P_{BESS,4}$ reaching 91 kW at t = 60 s. However, as PV generation reaches its maximum level and the global dispatch requirement for EC_4 is curtailed at t = 240 s, the controller intelligently reverses the BESS operation. The EC shifts from discharging to high-rate charging, reaching −97 kW to store solar excess. This ensures that P_4 is precisely reduced to 75 kW. Conversely, the FL-PSO response in Fig. 6h fails to exploit this bidirectional potential effectively. Its BESS output remains in a positive discharge state for the majority of the simulation. Consequently, the FL-PSO manages a slow

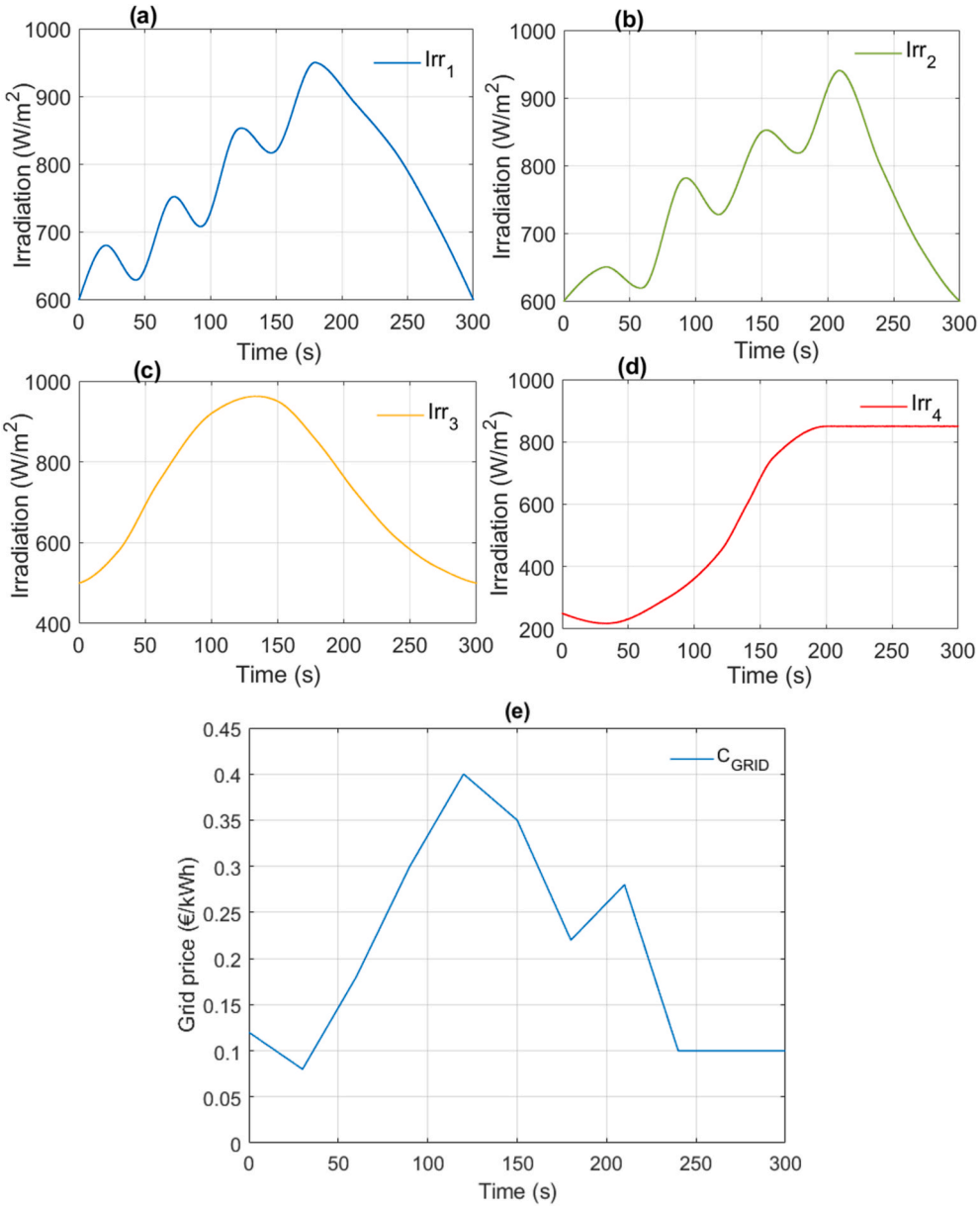

Fig. 5. Irradiation profiles: (a) EC_1, (b) EC_2, (c) , EC_3 , (d) EC_4, (e) C_{GRID}

gradual ramp in P_4 from an initial 99 kW to a peak of 170 kW and finishes at 103 kW. Therefore, it fails to emulate the decisive step-responses and efficient energy harvesting exhibited by the FL-AMPC, which precisely adapts the delivered power in scenarios where it is required.

Collectively, Fig. 6 serves two critical purposes. First, it confirms the correct operation of the four PV plants, which flawlessly track their MPPs under the incident irradiance. More significantly, it demonstrates the crucial role of the BESS as an active regulating asset. In each case, the BESS smooth the inherent volatility of the RETs, enabling each EC to operate as a fully dispatchable, reliable unit. The heterogeneous nature of these four distinct operational scenarios underscores the complexity of the testbed, providing a rigorous environment for evaluating the coordination performance of the proposed FL-AMPC.

Fig. 7 provides a critical insight into the intelligent power dispatch strategy of the FL-AMPC, illustrating the allocated power for each EC (P_i) in relation to its dynamic available power (P_i^{ava}). A fundamental operational constraint, rigorously enforced by the controller at all times, is that the injected power must never exceed this available capacity. This constraint gives rise to a critical trade-off. Suppose an EC with a high available capacity operates very close to this limit. In that case, it faithfully maximises renewable energy utilisation, but incurs significant associated power losses. The following analysis demonstrates the performance of the FL-AMPC and the FL-PSO.

The results for EC_1 highlight contrasting levels of tracking fidelity. In Fig. 7a, the FL-AMPC ensures that P_1 adheres strictly to P_1^{ava} boundary, oscillating between 255 kW and 300 kW and achieving a final value of 215 kW. By operating at the limit, the controller prioritises total energy contribution over loss minimisation. In contrast, the FL-PSO (Fig. 7b) keeps P_1 at a lower level, ranging from 200 kW to 250 kW, resulting in a lower RETs use while, at the same time, reduce the overall losses.

The strategic superiority of the FL-AMPC is most evident in the operational transitions of EC_2. As shown in Fig. 7c, the controller manages P_2 through three distinct phases: initial curtailment, intensive tracking, and final curtailment. For t < 60 s, the FL-AMPC deliberately keeps P_2 at 180 kW—well below the 290 kW available—to operate in a high-efficiency, low-loss operation mode. At t = 60 s, it executes a sharp step-response to 320 kW to meet a specific system demand, tracking P_2^{ava} exactly. Once the demand eases, it immediately reverts to the lower-loss

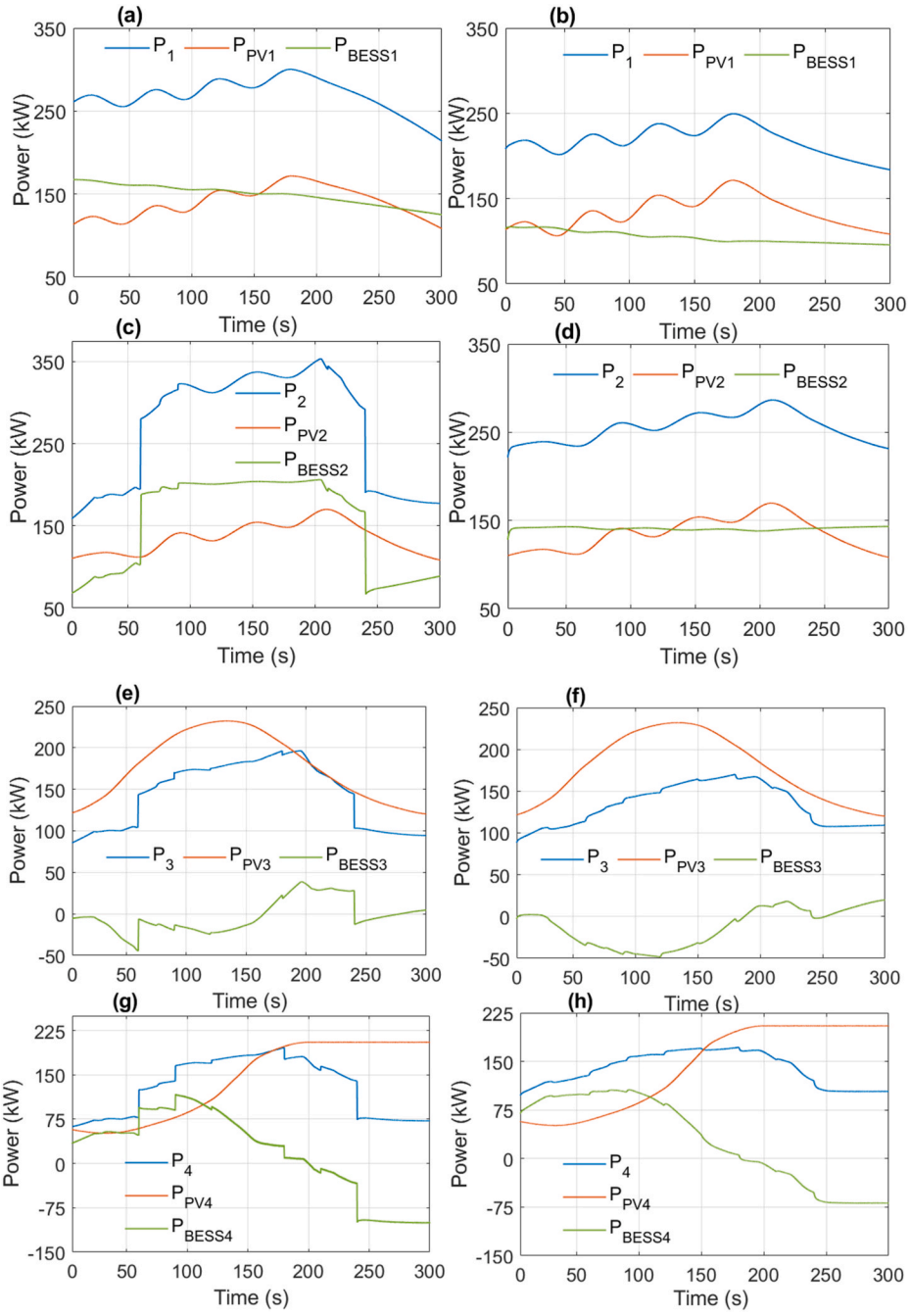

Fig. 6. EC internal power: (a) FL-AMPC EC_1: P_1, $P_{PV,1}$, $P_{BESS,1}$, (b) FL-PSO EC_1: P_1; $P_{PV,1}$; $P_{BESS,1}$, c) FL-AMPC EC_2: P_2, $P_{PV,2}$, $P_{BESS,2}$, (d) FL-PSO EC_2: P_2; $P_{PV,2}$; $P_{BESS,2}$, e) FL-AMPC EC_3: P_3, $P_{PV,3}$, $P_{BESS,3}$, (f) FL-PSO EC_3: P_3; $P_{PV,3}$; $P_{BESS,3}$, g) FL-AMPC EC_4: P_4, $P_{PV,4}$, $P_{BESS,4}$, (h) FL-PSO EC_4: P_4, $P_{PV,4}$, $P_{BESS,4}$.

regime at 175 kW. In stark contrast, the FL-PSO (Fig. 7d) is unable to perform such selective dispatch; it merely follows the solar shape, remaining confined between 230 kW and 280 kW. This evidence the superior performance of the FL-AMPC, moving the operation in accordance with the IEEE-15 bus network requirements.

The trajectories for EC_3 operate under an available power limit (P_3^{ava}) that follows a bell-shaped profile, peaking at 350 kW around t = 130 s. In Fig. 7e, the FL-AMPC manages P_3 through distinct operational shifts, featuring a step-increase to 145 kW at t = 60 s and a sharp reduction back to a 100 kW at t = 240 s. Between these transitions, the delivered power reaches a peak of 200 kW. In contrast, the FL-PSO (Fig. 7f) maintains a smoother, continuous trajectory without discrete steps. Its output P_3 reaches a lower peak of 170 kW and settles at a 108 kW level during the final stage. Notably, both controllers maintain a substantial offset from the P_3^{ava} limit in this scenario, prioritising a lower-loss regime.

A similar behaviour is observed in EC_4, where P_4^{ava} exhibits a notably increment, reaching 310 kW after t = 200 s. As shown in Fig. 7g, the FL-AMPC enforces a decisive power step at t = 60 s, subsequently ramping P_4 from 130 kW to a peak of 200 kW. At t = 240 s, the controller executes a sharp downward step to a stable 75 kW. Conversely, the FL-PSO (Fig. 7h) transitions more gradually throughout the 300 s window. Its delivered power P_4 peaks at 175 kW and settles at a higher final of 103 kW. The quantitative benefits of the FL-AMPC, predictive power distribution, which leverages the rolling-horizon methodology for dynamic power control, will be analysed in detail in the subsequent section.

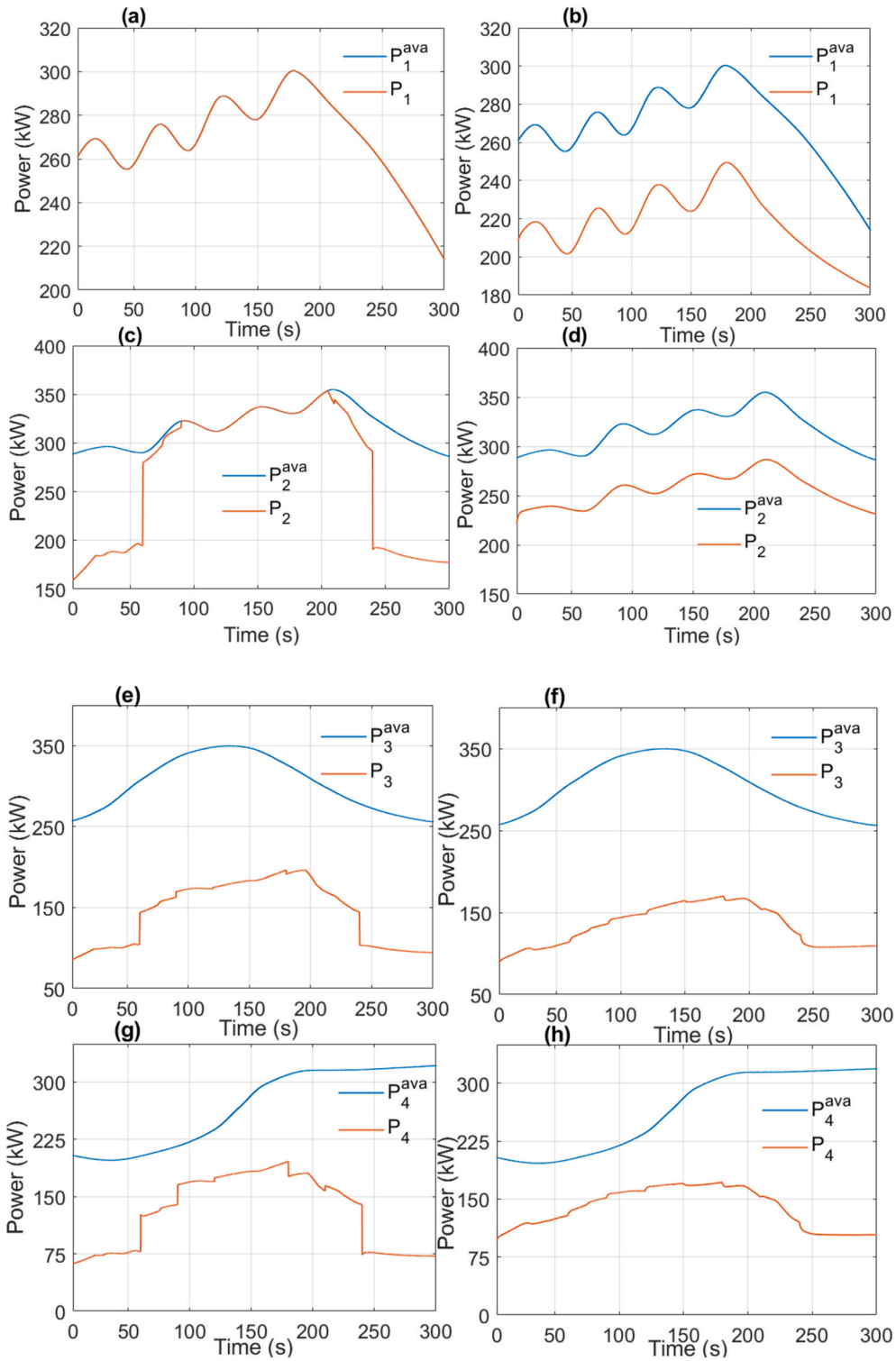

Fig. 7. EC capacity and delivered power: (a) FL-AMPC EC_1: P_1^{ava} and P_1, (b) FL-PSO EC_1: P_1^{ava} and P_1, c) FL-AMPC EC_2: P_2^{ava} and P_2, (d) FL-PSO EC_2: P_2^{ava} and P_2, e) FL-AMPC EC_3: P_3^{ava} and P_3, (f) FL-PSO EC_3: P_3^{ava} and P_3, g) FL-AMPC EC_4: P_4^{ava} and P_4, (h) FL-PSO EC_4: P_4^{ava} and P_4.

5.2. Comparative analysis of power distribution profiles

The systemic coordination of power distribution within the ECs under dynamic operational conditions is delineated in Fig. 8. The power profiles for the proposed FL-AMPC and the FL-PSO benchmark are depicted in Fig. 8a and b, respectively. Both controllers are required to satisfy the complex, multi-layered demand profile shown in Fig. 8c, which integrates a passive load ($P_{PASSIVE}$), dispatchable loads subject to demand-side management (P_{DSM}). Furthermore, the reserve power is also depicted to complete the power balance and clarify the variations in P_{DSM}.

The following analysis provides an exhaustive comparison of the divergent trajectories produced by both controllers across three critical temporal windows, highlighting the impact of the adaptive approach on EC efficiency and cleaner demand fulfilment.

P_{TOTAL} initiates at approximately 784 kW and climbs to a peak of

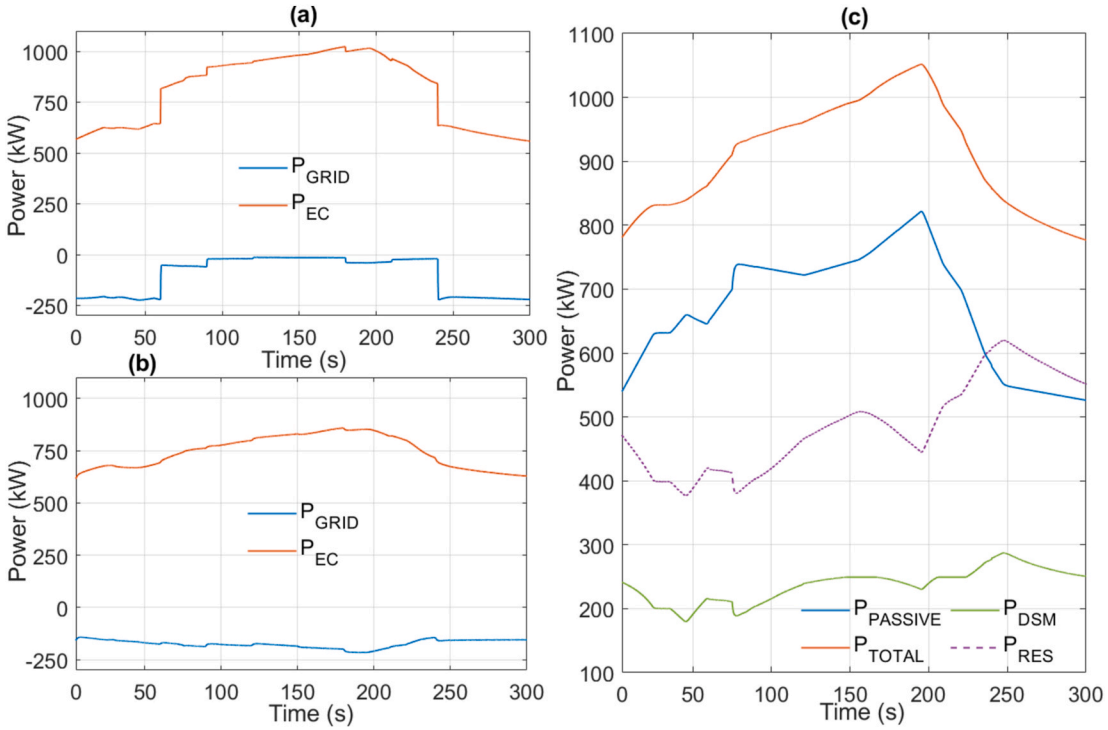

Fig. 8. ECs power dispatch: (a) FL-AMPC P_{GRID} and P_{EC}, (b) FL-PSO P_{GRID} and P_{EC} (c) and (c) total demand (P_{TOTAL}), passive demand (P_{GRID}), controllable demand (P_{DSM}) and reserve power (P_{DSM}).

1052 kW at t = 196 s, driven by a rigid $P_{PASSIVE}$ that fluctuates between 542 kW and 821 kW, and a dispatchable component under demand-side management, averaging 240 kW. Furthermore, P_{RES}, which varies between 378 kW and 620 kW, is visualised to complete the power balance. Crucially, the dispatch logic is intrinsically linked to the extreme grid price volatility established in Fig. 5e, where C_{GRID} surges from 0.08 €/kWh to 0.40 €/kWh.

During the initial scenario, from 0 to 60 s, characterised by a low-cost regime in the primary grid energy price (0.08–0.12 €/kWh), P_{TOTAL} rises from 784 kW to 852 kW. In this interval, the FL-AMPC (Fig. 8a) maintains the aggregate EC power (P_{EC}) between 569 kW and 643 kW, consciously opting for a managed primary grid import (P_{GRID}) of approximately −220 kW. This strategy demonstrates an intelligent allocation of energy resources, aiming to cost optimisation and taking advantage of the low price of the primary grid. However, the high power imported from the primary grid results in low RET usage, as discussed in the subsequent section. The FL-PSO (Fig. 8b) exhibits a similar performance in this scenario, with a lower level of power imported from the primary grid, ranging from −145 kW to −175 kW.

Crucial evidence of the FL-AMPC's superiority occurs during the high-price mitigation window, between 60 and 240 s. As C_{GRID} initiates its steep ascent toward 0.40 €/kWh, the FL-AMPC executes an instantaneous, high-fidelity step-response. To compensate for a P_{TOTAL} that reaches its maximum of 1052 kW (where $P_{PASSIVE}$ is 821 kW and P_{DSM} is 231 kW), the FL-AMPC elevates P_{EC} to a peak of 1020 kW. This rapid mobilisation of local RETs acts as a "financial shield", driving P_{GRID} to a near-zero exchange state precisely when the primary grid is most expensive. This operation implies two important consequences. First, because the ECs mostly meet demand, the RETs' usage level increase. However, a second conclusion derived from this, is that the power losses are incremented due precisely to the higher reliance on local ECs. In stark contrast, the FL-PSO is hindered by multi-objective optimisation; it fails to execute a discrete dispatch shift, merely following a lower ramp that only reaches 850 kW at t = 120 s. This leaves a 170 kW deficit compared to the P_{TOTAL} requirements, forcing the ECs to continue importing expensive energy at a rate of −180 kW, incurring a significant financial penalty.

The final transition at t = 240 s further underscores the adaptive intelligence of the proposed framework, as the price drops to 0.10 €/kWh. The FL-AMPC demonstrates immediate economic optimisation, dropping P_{EC} back to the 600 kW power dispatch despite P_{TOTAL} still being around 830 kW. This allows the ECs to instantaneously resume primary grid imports when they are cost-effective, thereby reducing the use of internal resources. Simultaneously, the FL-PSO continues to import power from the primary grid due to economic considerations. While both controllers technically satisfy the multi-component load requirements (Fig. 8c), the superiority of the FL-AMPC stems from its ability to perform instantaneous multi-objective adaptability. Unlike the FL-PSO, which relies on a rigid heuristic search that attempts to satisfy all objectives simultaneously, the adaptive framework operates within a dynamic adaptability. By allocating power flows at every discrete control interval based on the current marginal cost of the primary grid and total demand, the FL-AMPC can dynamically shift its priority from resource preservation to aggressive cost mitigation when economic conditions fluctuate.

The outcomes illustrated in Fig. 8 confirm that the FL-AMPC achieves a state of active economic decoupling. Where the FL-PSO remains as a multi-objective optimisation that allows to fulfil the demand and establish an optimal power distribution, the adaptive framework functions as a proactive energy orchestrator. By leveraging its predictive horizon to anticipate price gradients and mobilise internal flexibility (C_{GRID} and P_{RES}), the proposed FL-AMPC ensures that the ECs are not merely balanced, but economically more favourable. This capability to execute precise, point-in-time decisions ensures that the EC's operation is optimised for the specific reality of each moment rather than settling for a compromised, static optimum.

Following the qualitative demonstration of the controller's adaptive behaviour, Fig. 9 provides the assessment of the FL-AMPC framework's performance. To this end, the adaptive weights derived from the FL supervisor are shown. The core of the framework's intelligence is depicted in the dynamic evolution of the adaptive weights (w_{LOAD}; w_{COST}; w_{LOSS}, w_{USE}) that govern the AMPC's objective function. During

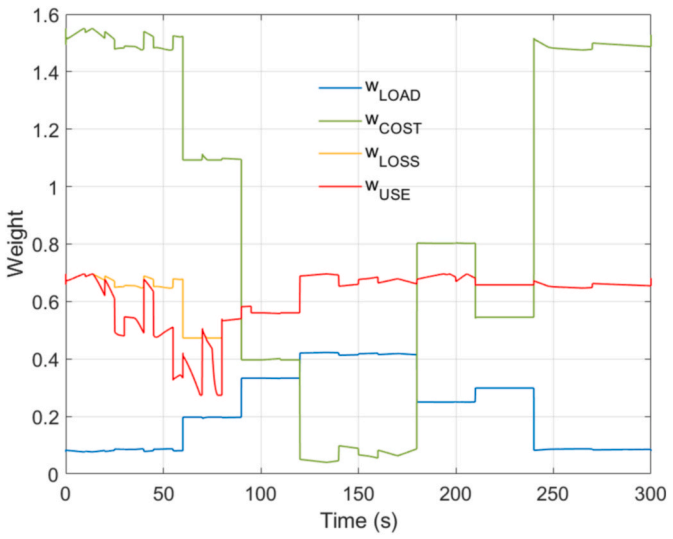

Fig. 9. FL-AMPC weights: self-sufficiency (w_{LOAD}), cost (w_{COST}), losses (w_{LOSS}), RETs use (w_{USE}).

periods of low grid prices, such as the initial interval from t = 0s to t = 60s, the FL supervisor executes a clear economic strategy: it aggressively elevates the cost weight (w_{COST}) while simultaneously suppressing the self-sufficiency weight (w_{LOAD}). This action explicitly commands the AMPC to prioritise cheap grid power. However, as the grid price rises, a strategic inversion occurs.

The value of w_{COST} is progressively diminished in favour of w_{LOAD}, which ascends to dominance and peaks at t = 150s, perfectly coinciding with the most expensive grid prices. This forces the AMPC to shift its priority towards autonomy. As the grid price recedes in the final operational phase, w_{LOAD} decreases and w_{COST} is once again elevated, guiding the system back to an economically optimal state. Throughout this entire process, the weights for losses (w_{LOSS}) and RET utilisation (w_{USE}) maintain a persistent, balanced tension, ensuring that neither objective is completely sacrificed in pursuit of the primary goal.

5.3. Quantitative evaluation of sustainable process improvements

The transition towards a cleaner, low-carbon modern power system requires ECs to operate not only for technical stability but also with a focus on resource efficiency and waste minimisation. To satisfy the pillars of sustainable production, the proposed system is evaluated through an exhaustive analysis of four critical indicators: operational expenditure (OPEX) as a proxy for resource management; power loss reduction (waste mitigation); maximising RET utilisation; and the corresponding mitigation of CO_2 emissions. This final metric is intrinsically linked to the ECs' grid dependency. To this end, while reducing reliance on the primary grid, the ECs effectively avoid the carbon emissions associated with the primary grid's energy mix.

To provide a rigorous environmental validation, the carbon impact is quantified by considering the proportion of non-renewable sources present in the external supply. The calculation is based on the projected electric mix of the Spanish electricity market for 2025. Specifically, an annual average emission factor of 133.583 g CO_2/kWh is utilised, derived from a detailed analysis of monthly data from the Spanish national power system (Real-time CO2 emissions from electricity). Consequently, any reduction in primary grid energy reliance achieved by the FL-AMPC is directly translated into a quantifiable decrease in the EC's carbon footprint, as local renewable generation displaces the need for carbon-intensive grid imports.

By examining these metrics, this analysis demonstrates how integrating predictive-adaptive logic transforms the EC from a passive energy consumer into an agile, eco-efficient production unit.

The cost architecture is illustrated in Fig. 10, which provides a comparative breakdown of the internal operational costs for the FL-AMPC (Fig. 10a) and the FL-PSO (Fig. 10b). The total price is dissected into internal unit expenditures ($C_{EC,1}$ to $C_{EC,4}$), primary grid purchased costs (C_{GRID}), and costs associated with losses (C_{LOSS}). As evidenced in the trajectories, a primary indicator of cleaner production is the reduction in power losses. The FL-AMPC (Fig. 10a) achieves a streamlined loss profile, maintaining C_{LOSS} values between 4.1 €/h and 7.8 €/h. Conversely, the FL-PSO benchmark (Fig. 10b) exhibits higher dissipation, with C_{LOSS} values rising more aggressively, peaking at approximately 8.2 €/h. This confirms that the adaptive-predictive logic achieves superior performance in local power flows, thereby maximising global efficiency.

The most significant process improvement is observed in the strategic management of primary grid interactions during high-price intervals, from 60 s to 240 s. While the FL-PSO (Fig. 10b) remains heavily reliant on the primary grid, with C_{GRID} values surging from a baseline of 30 €/h to a maximum of 83.1 €/h during the peak window, the FL-AMPC (Fig. 10a) executes an immediate and sustained economic decoupling. The proposed framework drives the C_{GRID} component down to a controlled range between 5.8 €/h and 10.2 €/h during the same peak interval. This agility is not merely a financial advantage but a vital decarbonisation mechanism to avoid reliance on the primary grid, which is partially powered by non-renewable generation technologies.

The aggregate impact of these sustainable process improvements is consolidated in Fig. 10c, where the divergent cumulative cost trajectories highlight the advantages of the adaptive framework. Throughout the simulated period, the FL-PSO maintains an average operational cost of 130.4 €/h, largely driven by the cumulative effect of its delayed reaction to market signals and the subsequent reliance on expensive grid procurement. In contrast, the FL-AMPC achieves a significantly lower mean operational expenditure of 109.1 €/h. This consistent reduction in average costs results in a 19.52% reduction. It is a direct consequence of the proposed approach's capability to execute precise, point-in-time reconfigurations, ensuring that local renewable resources are maximised and energy waste is curtailed. Ultimately, the results substantiated in Fig. 10 confirm that the FL-AMPC transcends standard balancing tasks and fulfils the core principles of cleaner production by aligning long-term economic viability with rigorous environmental stewardship.

The environmental dimension of this process improvement is quantified by evaluating the CO_2 emissions intrinsically linked to grid dependency. Given the projected average emission factor of 133.583 g CO_2/kWh (Real-time CO2 emissions from electricity), the carbon footprint is determined by the total energy imported (E_{GRID}) from the primary grid. E_{GRID} is calculated as the time integral of the grid power exchange (P_{GRID}). Over the entire simulation, the FL-PSO requires a total energy import from the primary grid of 14.6 kWh, resulting in an aggregate CO2 emission of 1950.32 g. In contrast, the proposed FL-AMPC leverages its predictive horizon to displace carbon-intensive imports strategically, reducing the required energy procurement to only 8.5 kWh. This translates to a significantly reduced environmental impact of 1135.45 g CO_2, representing a substantial 41.78% reduction in the EC's carbon footprint. This reduction in energy procurement from the primary grid constitutes a direct environmental improvement for the FL-AMPC. By minimising reliance on the grid, the proposed framework ensures lower operational costs alongside a significant decrease in CO_2 emissions. This link between reduced energy imports and lower carbon intensity provides a clear, quantifiable justification for why the FL-AMPC is a superior tool for cleaner, sustainable production compared to traditional control methods.

Finally, to complement the economic and environmental assessment, Fig. 11 illustrates power losses and RET utilisation for both control strategies. In Fig. 11a, the FL-AMPC maintains a consistently lower power loss profile, starting at 12.1 kW, compared to the 15.8 kW dissipated by the FL-PSO. Throughout the simulation, the FL-AMPC achieves a mean loss of 21.01 kW, while the FL-PSO averages 22.77

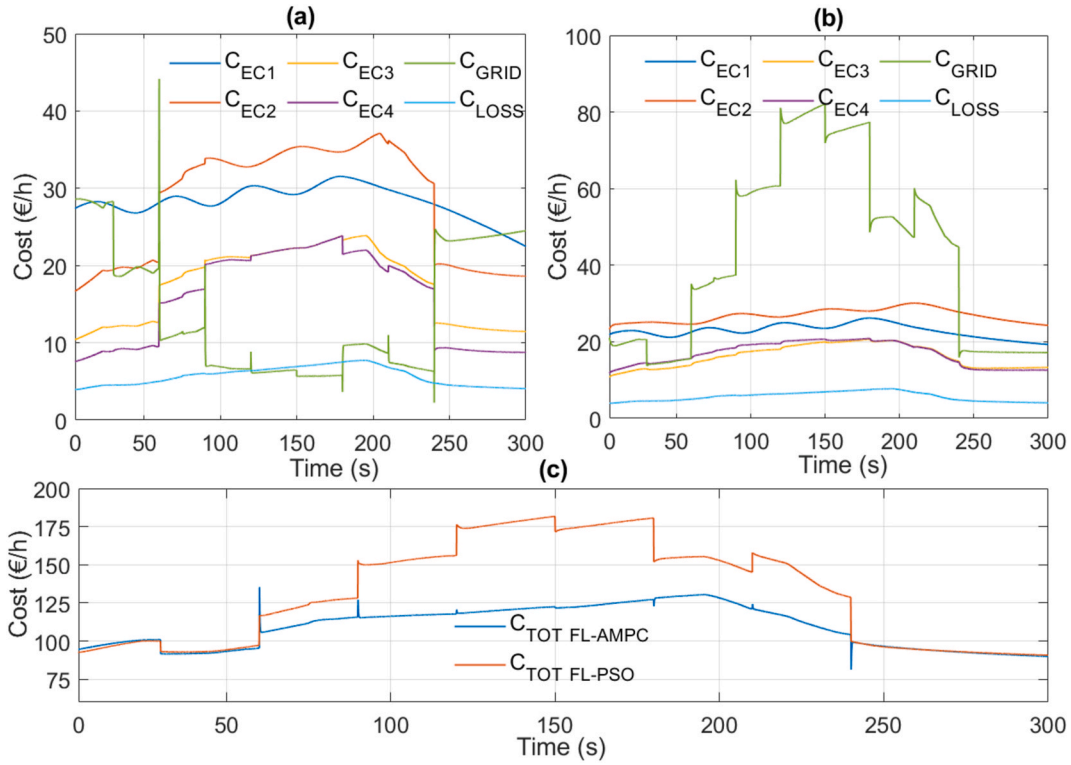

Fig. 10. EC operating costs: (a) FL-AMPC EC cost (C_{EC}), grid cost (C_{GRID}) and losses cost (C_{LOSS}), (b) P_{EC}, (b) FL-PSO EC cost (C_{EC}), grid cost (C_{GRID}) and losses cost (C_{LOSS}) and (c) FL-AMPC total cost ($C_{TOT\ FL-AMPC}$) and FL-PSO total cost ($C_{TOT\ FL-PSO}$)

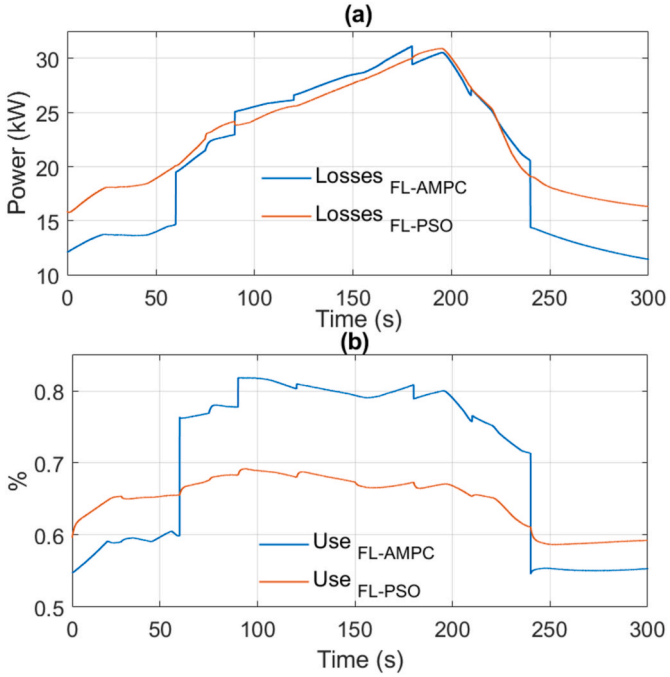

Fig. 11. EC loss and RETs usage: (a) FL-AMPC EC and FL-PSO power loss and (b) FL-AMPC and FL-PSO RETs usage.

kW, representing a 8.38% reduction in energy waste.

Furthermore, Fig. 11b confirms the superior management of local resources through a clear strategic shift. During the high grid-dependency intervals, from 0 to 60 s and from 240 to 300 s, the RETs' utilisation predictably decreases as the system relies on external procurement. However, during the critical window from 60 to 240 s, when the FL-AMPC prioritises the ECs' internal resources, the RETs' usage increases considerably, significantly outperforming the FL-PSO. Overall, the proposed approach increases the mean RET utilisation to 69.77%, compared with the benchmark's 64.52%. This 7.52% improvement confirms that the predictive-adaptive logic effectively maximises local green generation precisely when it is most needed to displace carbon-intensive grid imports.

In essence, the quantitative comparison reveals a crucial distinction in the methodology's intelligence. Both frameworks are designed to solve the same multi-objective problem. The FL-PSO approaches this challenge by seeking a compromised solution—a static balance between competing objectives. The proposed FL-AMPC, however, demonstrates a higher level of operational intelligence. It understands that while the overall goal is the same, the optimal strategy for achieving it is not. Its defining advantage is the ability to arbitrage between these objectives dynamically, prioritising cost savings when grid prices are low and enforcing self-sufficiency when they are high. This is not a redefinition of the problem, but a more sophisticated method of solving it—one that executes the right strategy at the right time, rather than settling for a single, compromised strategy for all the time. Taken together, these four KPIs highlight a clear distinction in operational philosophy. The FL-AMPC's superior performance stems from its predictive capabilities, which enable it to proactively seize economic opportunities and build resilience, rather than merely reacting to events. This approach results in a system that is demonstrably more cost-effective, more efficient, and significantly more autonomous. Table 6 presents the performance comparison between FL-AMPC and FL-PSO.

5.4. Comparative analysis with state-of-the-art approaches

To contextualise the outcomes of the proposed approach with similar findings from the current literature, this section presents a quantitative and qualitative comparison of the obtained results against recent studies in the field of ECs optimisation management. The comparison focuses on

Table 6
Comparative performance of FL-AMPC against PSO-EMS.

Parameter	Description	FL-AMPC	FL-PSO	Variation (%)
$C^{tot}_{op,k}$	Mean total cost (€/h)	109.1	130.4	−19.52
$P^{tot}_{loss,k}$	Mean total power generation losses (kW)	21.01	22.77	−8.38
U_{RET}	Mean utilisation factor (%)	69.77 %	64.52	+7.52
E_{CO2}	Equivalent CO_2 emissions (g CO_2)	1135.45	1950.32	−41.78

key performance indicators, such as operational cost reduction, CO_2e-missions mitigation, power losses, and the effective utilisation of RETs. Regarding economic efficiency, the proposed FL-AMPC approach achieved a mean total cost reduction of 19.52% compared to the FL-PSO baseline. In the broader literature, reported results vary significantly based on the specific constraints and market structures employed. For instance, reference (Silva et al., 2024) focused on cost minimisation. It utilised a hybridised ant colony optimisation and genetic algorithm, reporting a cumulative cost saving of 33.67%. In comparison, reference (Zeng and Yi, 2025) achieved a 31.2% reduction in a multi-vector integrated energy system using a modified approach. Although these heuristic approaches (Silva et al., 2024; Zeng and Yi, 2025) report higher nominal cost savings, they achieve these outcomes by relaxing complex grid dynamics and transient phenomena, which could compromise results in a real operational environment.

Conversely, when compared to frameworks that strictly prioritised carbon tracking or specific operational baselines, the proposed method demonstrates superior economic performance. For instance, the study in (Tan et al., 2024) reported an operational cost decrease of only 1.02%, and reference (Yang et al., 2019) focused on matching an ideal cost profile with a minimal increase of 0.4%, rather than an aggressive reduction. Therefore, the proposed approach offers a balanced trade-off, delivering substantial cost savings while maintaining rigorous physical grid constraints.

While the economic results are competitive, the most significant novelty and advantage of the proposed work lies in its environmental impact. The FL-AMPC framework achieved a 41.78% reduction in equivalent CO_2 emissions. This performance notably outperforms similar carbon-oriented studies found in the literature. For example, the mechanism proposed in (Tan et al., 2024), which employs a conditional value-at-risk method and carbon tracing to manage pollution, achieved a 0.66% decrease in daily total carbon. This stark contrast highlights the limitations of standard risk-based frameworks for achieving deep decarbonisation, compared to the predictive and adaptive nature of the proposed approach. This underscores the distinct advantage of the proposed FL-AMPC in effectively prioritising sustainability goals without compromising economic viability.

Complementing these environmental benefits, the proposed solution also excels in technical operation, specifically regarding power losses and RETs integration. The results show a 8.38% reduction in power generation losses and a 7.52% increase in the RET utilisation factor, simultaneously. In comparison, reference (Zabihinia Gerdroodbari et al., 2024), which utilised dynamic export limits and community ESS to manage congestion, reported a total generation increase of 4.6%. Consequently, the proposed approach demonstrates greater capability to enhance renewable integration. Moreover, regarding flexibility and imbalance (Ikuta and Aki, 2025), achieved 76% imbalance reduction using price-based DSM and (Yang et al., 2025) improved load matching through stochastic optimisation, respectively. While these studies (Ikuta and Aki, 2025; Yang et al., 2025) and peer-to-peer frameworks such as (Aminlou et al., 2024) achieved high performance in specific flexibility or trading tasks, they often overlooked the network's power losses. The proposed FL-AMPC provides a more holistic improvement, directly reducing losses while ensuring the system operates closer to its maximum renewable generation potential.

This comparative analysis reveals the distinct position of the proposed approach within the state of the art. While specific heuristic methods (e.g., (Silva et al., 2024), (Zeng and Yi, 2025)) may yield higher theoretical cost savings, they often lack the robustness to uncertainty that the proposed predictive control offers and do not consider the dynamic and transient states of ECs. Conversely, stochastic and risk-based models (e.g., (Tan et al., 2024), (Yang et al., 2025)) address uncertainty but often yield conservative improvements in emissions or generation efficiency. The novelty of the proposed FL-AMPC lies in its federated and predictive capability, allowing it to outperform the FL-PSO baseline across all metrics and surpass state-of-the-art values in emission reduction and RET utilisation, proving it to be a comprehensive solution for sustainable, efficient, and cost-effective ECs management.

6. Conclusions

This paper presented a novel FL-AMPC EMS framework designed to address the critical challenge of managing ECs in modern power grids under highly dynamic, uncertain conditions. The research was motivated by the inherent limitations of conventional control strategies, which often fail to navigate the complex, dynamic trade-offs between economic viability, technical efficiency, and resilient operation. The proposed framework was specifically designed to overcome this gap by introducing a higher level of operational intelligence, capable of dynamically arbitrating between these competing objectives.

The comprehensive comparative analysis conducted in this study provided a definitive validation of the proposed adaptive and predictive paradigm. When benchmarked against a state-of-the-art, non-predictive FL-PSO controller, the FL-AMPC demonstrated profound superiority across four KPIs. It achieved a substantial 19.52% reduction in operational expenditure, a direct consequence of its ability to proactively exploit low-cost grid opportunities and decisively enforce self-sufficiency during high-price events. This economic prowess was complemented by a compelling 8.38% reduction in power losses and a remarkable 41.78% decrease in equivalent CO_2 emissions, empirically proving the advantages of the proposed approach. These results underscored a fundamental distinction in control intelligence. The FL-PSO, while competent, was engineered to find a static, compromised solution to a fixed multi-objective problem. The proposed FL-AMPC, in contrast, demonstrated a more sophisticated capability: it understood that while the overall goal was fixed, the optimal strategy to achieve it was not. Its defining advantage lies in dynamically redefining the problem in real-time, elevating the priority of the most critical objective at any given moment. The fact that it achieved these gains while also securing a 7.52% improvement in the RETs utilisation factor proved that this was not a system of compromises, but one of synergistic optimisation. Furthermore, these findings challenged the adequacy of conventional EMS approaches that operate on coarse, minute-level time horizons.

By capturing the system's high-frequency dynamics at a microsecond resolution, this work demonstrated that significant economic and technical penalties are incurred when fast electromagnetic transients are neglected. The key innovation, therefore, lay not merely in adapting a system model to data, but in adapting the control objective itself to the prevailing operational context —a paradigm shift from reactive optimisation to proactive strategy. In conclusion, this work empirically demonstrated that a control architecture capable of intelligent, dynamic strategic arbitration is not merely an incremental improvement, but a necessity for the robust, efficient, and autonomous operation of the next generation of ECs.

Notwithstanding these significant advancements, the scope of the current framework presents certain limitations that warrant acknowledgement. Primarily, the study remains centred on the electrical domain of ECs. Therefore, the intricate dynamics associated with multi-energy configurations—such as thermal inertia, the variable coefficients of

performance in thermal assets, and the non-linear conversion efficiencies of hydrogen-based vectors—have not been explicitly considered. While these omissions do not detract from the fundamental conclusions regarding the controller's efficacy in electrical power dispatch, they define the current operational boundary of the proposed strategy. Assessing the impact of these limitations suggests that integrating thermal and gas-to-power coupling would likely provide additional degrees of freedom for the EMS, potentially further enhancing the economic and technical gains reported herein. Consequently, future research could be directed towards expanding the internal model of the AMPC to encompass these multi-vector interdependencies. This evolution could facilitate a more holistic arbitration of resources, ensuring that the strategic intelligence of the FL-AMPC framework remains robust within the increasingly integrated landscape of the next generation of ECs.

CRediT authorship contribution statement

Pablo Horrillo-Quintero: Writing – original draft, Visualization, Validation, Software, Resources, Methodology, Investigation, Formal analysis, Data curation, Conceptualization. **Pablo García-Triviño:** Writing – original draft, Visualization, Validation, Software, Resources, Methodology, Investigation, Formal analysis, Conceptualization. **Mohammad Sadegh Javadi:** Writing – original draft, Visualization, Validation, Resources, Methodology, Investigation, Conceptualization. **Luis M. Fernández-Ramírez:** Writing – review & editing, Writing – original draft, Visualization, Validation, Supervision, Project administration, Methodology, Investigation, Funding acquisition, Formal analysis, Conceptualization. **João P.S. Catalão:** Writing – review & editing, Methodology, Investigation, Formal analysis, Conceptualization.

Declaration of competing interest

The authors declare that they have no known competing financial interests or personal relationships that could have appeared to influence the work reported in this paper.

Acknowledgments

The research leading to these results has received partial financial support from the Ministerio de Ciencia, Innovación y Universidades, Agencia Estatal de Investigación, FEDER, UE (Grant PID2024-156036OB-C32 supported by MCIN/AEI/10.13039/501100011033/ FEDER, UE) and from the Consejería de Universidades, Investigación e Innovación de la Junta de Andalucía (Grant DGP_PIDI_2024_02368). The work of Pablo Horrillo-Quintero was partially supported by the Fundación Campus Tecnológico de Algeciras, with funding provided by the Consejería de Universidades, Investigación e Innovación de la Junta de Andalucía and the 'PLAN PROPIO-UCA 2025-2027' program. Moreover, Mohammad Sadegh Javadi and João P.S. Catalão acknowledge support from the EU Horizon Europe Programme under GA ID: 101230578 (INNO-TREC Project; DOI: 10.3030/101230578) and from COMPETE2030-FEDER-00883700 and FCT (INVINCIBLE Project; DOI: 10.54499/2023.17788.ICDT).

Data availability

Data will be made available on request.

References

Aittahar, S., de Villena, M.M., Derval, G., Castronovo, M., Boukas, I., Gemine, Q., et al., 2023. Optimal control of renewable energy communities with controllable assets. Front. Energy Res. 11. https://doi.org/10.3389/fenrg.2023.879041.

Aminlou, A., Mohammadi-Ivatloo, B., Zare, K., Razzaghi, R., Anvari-Moghaddam, A., 2024. Activating demand side flexibility market in a fully decentralized P2P transactive energy trading framework using ADMM algorithm. Sustain. Cities Soc. 100. https://doi.org/10.1016/j.scs.2023.105021.

Carraro, G., Dal Cin, E., Rech, S., 2024. Integrating energy generation and demand in the design and operation optimization of energy communities. Energies (Basel) 17. https://doi.org/10.3390/en17246358.

Chen, H., Zhang, L., Pinzon, S., Chen, H., Chen, B., 2025. Decarbonizing the G7: renewable energy, economic growth, globalization, and policy pathways to sustainability. Renew. Energy 244. https://doi.org/10.1016/j.renene.2025.122671.

Dimitroulis, P., Alamaniotis, M., 2022. A fuzzy logic energy management system of on-grid electrical system for residential prosumers. Elec. Power Syst. Res. 202. https://doi.org/10.1016/j.epsr.2021.107621.

Dorahaki, S., MollahassaniPour, M., Rashidinejad, M., Muyeen, S.M., Siano, P., Shafie-Khah, M., 2025. A robust optimization approach for enabling flexibility, self-sufficiency, and environmental sustainability in a local multi-carrier energy community. Appl. Energy 392. https://doi.org/10.1016/j.apenergy.2025.125997.

Fotopoulou, M., Tsekouras, G.J., Vlachos, A., Rakopoulos, D., Chatzigeorgiou, I.M., Kanellos, F.D., et al., 2025. Day ahead operation cost optimization for energy communities. Energies (Basel) 18. https://doi.org/10.3390/en18051101.

Habib, S., 2025. Robust load and energy management in smart grids with prosumer-integrated distributed energy resources. J. Clean. Prod. 496. https://doi.org/10.1016/j.jclepro.2025.145138.

Horrillo-Quintero, P., De la Cruz-Loredo, I., García-Triviño, P., Ugalde-Loo, C.E., Fernández-Ramírez, L.M., 2025. A real-time combined dynamic control framework for multi-energy microgrids coupling hydrogen, electricity, heating and cooling systems. Int. J. Hydrogen Energy 106, 454–470. https://doi.org/10.1016/j.ijhydene.2025.02.005.

Ikuta, K., Aki, H., 2025. Multi-timescale management models for distributed energy resources and a two-stage incentive design for demand-side grid flexibility provision. Sustain. Energy Grids Netw. 41. https://doi.org/10.1016/j.segan.2024.101618.

Kelepouris, N.S., Nousdilis, A.I., Bouhouras, A.S., Christoforidis, G.C., 2025. An energy management-based methodology for mutually beneficial interaction between prosumers and distribution system operator. Energy Convers. Manag. 346. https://doi.org/10.1016/j.enconman.2025.120433.

Lazzari, F., Mor, G., Cipriano, J., Solsona, F., Chemisana, D., Guericke, D., 2023. Optimizing planning and operation of renewable energy communities with genetic algorithms. Appl. Energy 338. https://doi.org/10.1016/j.apenergy.2023.120906.

Li, C., Jia, X., Zhou, Y., Li, X., 2020. A microgrids energy management model based on multi-agent system using adaptive weight and chaotic search particle swarm optimization considering demand response. J. Clean. Prod. 262. https://doi.org/10.1016/j.jclepro.2020.121247.

Ramirez-Marin, S.A., Garcés-Ruiz, A., Cortés-Borray, A.F., Perez-Basante, A., Rodríguez-Seco, J.E., 2025. Model-predictive control with admittance matrix estimation for the optimal power sharing in isolated DC microgrids. Elec. Power Syst. Res. 241. https://doi.org/10.1016/j.epsr.2024.111380.

Real-Time CO_2 Emissions from Electricity Consumption | Electricity Maps, Accessed: January. 15, 2026. [Online]. Available: https://app.electricitymaps.com/map/12mo/monthly, 20.

Rollo, A., Serafini, P., Aleotti, F., Cilio, D., Morandini, E., Moneta, D., et al., 2025. Load shifting and demand-side management in renewable energy communities: simulations of different technological configurations. Energies (Basel) 18. https://doi.org/10.3390/en18040872.

Sepehrzad, R., Yadav, M., Lazaroiu, G.C., Avramidis, I.I., Benitez, I.B., Di Somma, M., et al., 2026. A critical overview of local energy communities: state-of-the-art, real-life applications & challenges and tackling the academia-industry gap. Renew. Sustain. Energy Rev. 226. https://doi.org/10.1016/j.rser.2025.116165.

Shi, Z., Liang, F., Pezzuolo, A., 2024. Renewable energy communities in rural areas: a comprehensive overview of current development, challenges, and emerging trends. J. Clean. Prod. 484. https://doi.org/10.1016/j.jclepro.2024.144336.

Siano P, Dolatabadi M, Alhelou HH, Borghetti A. Multi-objective optimization for assessing trade-offs between energy sharing and ancillary services in local energy communities n.d. https://doi.org/10.17775/CSEEJPES.2025.01110.

Silva, B.N., Khan, M., Wijesinghe, R.E., Wijenayake, U., 2024. Meta-heuristic optimization based cost efficient demand-side management for sustainable smart communities. Energy Build. 303. https://doi.org/10.1016/j.enbuild.2023.113599.

Tan, J., Niu, J., Niu, Y., Wang, H., 2024. Carbon-oriented pricing scheme in digitalized power transmission networks utilizing carbon-driven demand response program under risk investigation. J. Clean. Prod. 459. https://doi.org/10.1016/j.jclepro.2024.142210.

Tan, Y., Xu, W., Xu, Z., Tong, R., Zhang, Y., 2025. A two-layer nested game for an active energy community including shared energy storage and multiple prosumers under renewable portfolio standards. Int. J. Electr. Power Energy Syst. 169. https://doi.org/10.1016/j.ijepes.2025.110748.

Vidal-Martínez, R., García-Martínez, J.R., Rojas-Galván, R., Álvarez-Alvarado, J.M., Gozález-Lee, M., Rodríguez-Reséndiz, J., 2025. A review of Mamdani, Takagi–Sugeno, and Type-2 fuzzy controllers for MPPT and power management in photovoltaic systems. Technologies 13. https://doi.org/10.3390/technologies13090422.

Vivas, F.J., Pajares, A., Blasco, X., Herrero, J.M., Segura, F., Andújar, J.M., 2025. A novel energy management system based on two-level hierarchical economic model predictive control for use in microgrid control. Energy Convers. Manag. X 26. https://doi.org/10.1016/j.ecmx.2025.101027.

Wang, Z., Zhou, L., Xiong, L., Yang, H., Wang, J., Huang, S., 2024. Parameter-adaptive distributed model-predictive control for islanded AC microgrids: privacy-preserving perspective. IEEE Trans. Smart Grid 15, 4424–4435. https://doi.org/10.1109/TSG.2024.3399233.

Yan, X., Gao, C., Francois, B., 2025. Multi-objective optimization of a virtual power plant with mobile energy storage for a multi-stakeholders energy community. Appl. Energy 386. https://doi.org/10.1016/j.apenergy.2025.125553.

Yang, X., Zhang, Y., He, H., Ren, S., Weng, G., 2019. Real-time demand side management for a microgrid considering uncertainties. IEEE Trans. Smart Grid 10, 3401–3414. https://doi.org/10.1109/TSG.2018.2825388.

Yang, S., Liu, Y., Lv, S., Tan, Q., Tan, Z., 2025. A study on two-stage stochastic optimization scheduling of electro-hydrogen microgrid system considering supply-demand cooperation strategies and improved income allocation model. J. Clean. Prod. 533, 146916. https://doi.org/10.1016/j.jclepro.2025.146916.

Zabihinia Gerdroodbari, Y., Khorasany, M., Razzaghi, R., Heidari, R., 2024. Management of prosumers using dynamic export limits and shared community energy storage. Appl. Energy 355. https://doi.org/10.1016/j.apenergy.2023.122222.

Zeng, X., Yi, J., 2025. Optimization and efficiency enhancement of multi-energy systems in integrated energy parks: a comprehensive analysis of adaptive strategies and dynamic management. J. Clean. Prod. 521. https://doi.org/10.1016/j.jclepro.2025.146204.

Zhang, C., Rezgui, Y., Luo, Z., Jiang, B., Zhao, T., 2024. Simultaneous community energy supply-demand optimization by microgrid operation scheduling optimization and occupant-oriented flexible energy-use regulation. Appl. Energy 373. https://doi.org/10.1016/j.apenergy.2024.123922.